Computational Study of the Mechanism and Product Yields in the Reaction Systems $C_2H_3 + CH_3 \rightleftarrows C_3H_6 \rightleftarrows H + C_3H_5$ and $C_2H_3 + CH_3 \rightarrow CH_4 + C_2H_2$

Stanislav I. Stoliarov,[†,§] Vadim D. Knyazev,*[,†,‡] and Irene R. Slagle[†]

Research Center for Chemical Kinetics, Department of Chemistry, The Catholic University of America, Washington, D.C. 20064, and National Institute of Standards and Technology, Physical and Chemical Properties Division, Gaithersburg, Maryland 20899

Received: November 5, 2001; In Final Form: April 29, 2002

The mechanism of the radical−radical reaction $C_2H_3 + CH_3$ (1) was studied by quantum chemical methods. The pathways of reaction channels observed in previous experimental studies, as well as those of other potential channels, were investigated. The results of the quantum chemical study and of the earlier experimental work were used to create a model of the chemically activated route ($C_2H_3 + CH_3 \rightleftarrows C_3H_6 \rightarrow H + C_3H_5$) of reaction 1. In this model, energy- and angular momentum-dependent rate constants are calculated using the RRKM method in combination with the microcanonical variational selection of the transition states. Pressure effects are described by solution of the master equation. Temperature and pressure dependences of the rate constants and product yields were investigated. The model was used to predict the rate constants and branching fractions of reaction 1 at temperatures and pressures outside the experimental ranges. The same model was used to analyze kinetics of two other reactions which occur on the same potential energy surface: the thermal decomposition of propene (2) and the reaction of H atom with allyl radical, $H + C_3H_5 \rightleftarrows C_3H_6 \rightarrow C_2H_3 + CH_3$ (3). The results demonstrate the increasing importance of the $CH_3 + C_2H_3$ channels in both reactions 2 and 3 at high temperatures (above ∼1500 K).

I. Introduction

Radical−radical cross-combination reactions constitute an integral part of the overall mechanisms of oxidation and pyrolysis of hydrocarbons.[1,2] Reactions of this type are difficult to study experimentally due to the high reactivity of the chemical species involved and, consequently, reliable experimental data are sparse. Unlike the simple reactions of recombination of alkyl radicals that proceed via formation of stable molecules, cross-radical reactions that involve unsaturated species can possess complex mechanisms including chemically activated rearrangements and decomposition. Such reactions are characterized by complex distributions of products displaying both temperature and pressure dependences.

The reaction between vinyl and methyl radicals

$$C_2H_3 + CH_3 \rightarrow \text{products} \qquad (1)$$

is the simplest of the class of reactions between alkenyl and alkyl radicals. This reaction plays an important role in mechanisms of evolution of planetary atmospheres.[3,4] Both the methyl and the vinyl radicals are also critical intermediates in oxidation and pyrolysis of hydrocarbons.

The kinetics of reaction 1 has been studied experimentally by several groups. Fahr et al.[5,6] determined the rate constants of two reaction channels at room temperature and 13.3 kPa (100 Torr) of He and 13.3−39.9 kPa (100−300 Torr) of He and Ar using laser photolysis of methyl vinyl ketone as the source of both CH_3 and C_2H_3 radicals

$$C_2H_3 + CH_3 \rightarrow CH_2CHCH_3 \qquad k = (1.2 \pm 0.3) \times 10^{-10}\ \text{cm}^3\ \text{molecule}^{-1}\ \text{s}^{-1}$$

$$\rightarrow CH_4 + C_2H_2 \qquad k = (0.34 \pm 0.07) \times 10^{-10}\ \text{cm}^3\ \text{molecule}^{-1}\ \text{s}^{-1}$$

The rate constants were derived by monitoring the real-time kinetics of CH_3 decay and C_4H_6 formation using UV absorption spectroscopy, gas chromatographic end-product analysis, and detailed modeling of the kinetic mechanism.

More recently, experimental studies of reaction 1 were reported by three groups.[7−9] In our experimental work,[7] overall rate constants and product yields of reaction 1 were determined in the temperature region 300−900 K and bath gas (He) density $(3-12) \times 10^{16}$ molecule cm^{-3}. Kinetics of the C_2H_3 and CH_3 decay and that of product formation were monitored in real-time direct experiments using Laser Flash Photolysis/Time-Resolved Photoionization Mass Spectrometry. Three major reaction product channels were determined

$$C_2H_3 + CH_3 \rightarrow C_3H_6 \qquad (1a)$$

$$\rightarrow H + C_3H_5 \qquad (1b)$$

$$\rightarrow CH_4 + C_2H_2 \qquad (1c)$$

The relative importance of channels 1a−1c depended on temperature and pressure with channels 1a and 1b displaying negative and positive temperature dependences, respectively. The overall rate constant of reaction 1 decreased with temper-

* To whom correspondence should be addressed. E-mail: knyazev@cua.edu.

† Research Center for Chemical Kinetics, Department of Chemistry, The Catholic University of America.

‡ National Institute of Standards and Technology, Physical and Chemical Properties Division.

§ Current address: Department of Chemical Engineering, University of Massachusetts, Amherst, MA 01003.

10.1021/jp014059j CCC: $22.00
Published on Web 07/04/2002

ature and could be represented with the expression

$$k_1(T) = 5.1 \times 10^{-7} T^{-1.26} \exp(-362/T)\ \mathrm{cm^3\ molecule^{-1}\ s^{-1}} \quad \text{(I)}$$

No pressure dependence of the overall rate constant was observed within the experimental pressure range. The room-temperature rate constant value reported in our study ($k_1 = 1.18 \pm 0.16) \times 10^{-10}$ cm^3 molecule^{-1} s^{-1}) is between those reported by Fahr et al.[5,6] ($(1.5 \pm 0.3) \times 10^{-10}$ cm^3 molecule^{-1} s^{-1}) and by Thorn et al.[8] ($(1.02 \pm 0.53) \times 10^{-10}$ cm^3 molecule^{-1} s^{-1}) with the uncertainty limits of all three studies overlapping. Thorn et al.[8] used discharge flow/electron impact ionization mass spectrometry to study reaction 1 at room temperature and a pressure of 133 Pa (1 Torr).

The product distribution reported in our experimental work[7] is in agreement with the results reported in refs 8 and 9. Thorn et al.[8] qualitatively observed formation of C_3H_6, C_3H_5, and C_2H_2 as primary products of reaction 1 at 133 Pa (1 Torr). Fahr et al.[9] studied reaction 1 at room temperature and pressures 0.28−27 kPa (2.1−200 Torr) using laser photolysis of methyl vinyl ketone and final product analysis (gas chromatography and mass spectrometry). These authors have reported the reduction of the branching fraction of the C_3H_6 forming channel from 78% at high pressures to ∼39% at the low-pressure end of the experimental interval. At low pressures, the formation of 1,5-hexadiene and other products absent at high pressures was observed. This observation was interpreted by the authors as indicating the appearance of the reaction channel 1b at low pressures. The fraction of the C_3H_6 forming channel was determined from the ratios of concentrations of C_3H_6 and C_2H_6 products and the rate constant of methyl radicals recombination. Secondary reactions had a minor influence on the $[C_3H_6]/[C_2H_6]$ ratio and had to be accounted for via kinetic modeling.

The analysis of all of the experimental data on reaction 1 compelled the authors of refs 7−9 to conclude that the mechanism of reaction 1 consists of two processes: (1) addition with the formation of chemically activated propene, which can stabilize in collisions with the bath gas or decompose to H atom and allyl radical (reaction channels 1a and 1b) and (2) disproportionation where CH_3 radical abstracts a hydrogen atom from the vinyl resulting in product channel 1c

$$C_2H_3 + CH_3 \rightarrow CH_3CHCH_2^* \rightarrow CH_2CHCH_2 + H \quad \text{(1b)}$$

$$\downarrow [M]$$

$$CH_3CHCH_2 \quad \text{(1a)}$$

$$C_2H_3 + CH_3 \rightarrow CH_4 + C_2H_2 \quad \text{(1c)}$$

Fahr et al.[9] and Thorn et al.[8] performed modeling of the chemically activated route of reaction 1. Models used in these two articles were identical. Properties of critical transition states were selected to conform to the literature (experimental or calculated) temperature dependences of the high-pressure-limit rate constants. No variational effects or effects of angular momentum conservation were considered. Steady-state solution of the master equation[10] was used to describe collisional stabilization effects. The results of modeling indicated that the experimental results of Fahr et al. on the room-temperature pressure dependence of the $[C_3H_6]/[C_2H_6]$ ratio can be approximately reproduced by the model using the average energy transferred per deactivating collision with the bath gas $\langle \Delta E \rangle_{\mathrm{down}} = 400$ cm^{-1}. No attempt was made to use this model for extrapolation of the experimental results beyond the experimental range of conditions.

Although the product distribution of reaction 1 has been determined quantitatively as a function of temperature and pressure,[7] these experiments were conducted under conditions that are still far from the actual conditions of combustion: at low pressures and at $T \leq 900$ K. Major extrapolation based on the theory of unimolecular reactions is required to predict overall rate constants and product branching fractions at higher temperatures and pressures. The particular system of reaction 1 presents a challenge from the point of view of practical application of theory. Both addition reactions of C_2H_3 to CH_3 and of H atom to C_3H_5 (the reverse of decomposition of propene to the products of channel 1b) are barrierless and, therefore, variational selection of the transition state and explicit accounting for the effects of angular momentum conservation are needed to compute the microcanonical rate constants $k(E,J)$.[11−13] Collisional effects in the chemically activated reaction are best accounted for by a solution of master equation using the weak collision model. The current study has as one of its main goals the modeling of reaction 1, including the prediction of rates and product distributions as functions of temperature and pressure.

Several qualitative aspects of the mechanism of reaction 1 are still not resolved by the results of the experimental studies of refs 5−9. Although the most likely mechanism for the formation of the products of channel 1c, C_2H_2 and CH_4, is the direct abstraction (disproportionation), production of these species in a chemically activated rearrangement-decomposition cannot be excluded on the basis of experimental data alone. Also, other potential products of reaction 1 such as C_3H_4 (allene, propyne, or cyclopropene) + H_2, although not observed in experiments, cannot be ruled out completely. A possibility remains that these potential product channels have nonzero minor branching fractions (below the experimental detection level) but become important in the combustion environment.

In the current work, the mechanism of reaction 1 is studied by quantum chemical methods. In particular, the pathways of reaction channels 1a, 1b, and 1c, as well as other potential channels, are investigated. The results of the ab initio study and of the earlier experimental work are used to create a model of the chemically activated route in reaction 1 (channels 1a and 1b). In this model, energy and angular momentum dependent rate constants $k(E,J)$ are calculated using the RRKM method[11−14] in combination with the microcanonical variational selection of the transition state.[11−13] Pressure effects are described by the solution of the master equation using the approach described by Bedanov et al.[15] and the *virtual components* algorithm of Knyazev and Tsang.[16] Qualitative behavior of the calculated pressure dependences and the sensitivity of the modeling results to the critical parameters of the model are investigated. The model is used to predict the rate constants and branching fractions of reaction 1 at temperatures and pressures outside of the experimental ranges.

This same model is used to analyze the kinetics and product distributions of two other important reactions which occur on the same potential energy surface: the thermal decomposition of propene[17]

$$CH_3CHCH_2 \rightarrow H + CH_2CHCH_2 \quad \text{(2)}$$

$$\rightarrow CH_3 + C_2H_3$$

and the reaction of H atom with allyl radical

$$H + CH_2CHCH_2 \rightarrow CH_3CHCH_2 \quad \text{(3)}$$

$$\rightarrow CH_3 + C_2H_3$$

TABLE 1: Experimental Enthalpies of Formation of Reactants and Potential Products of the $C_2H_3 + CH_3$ Reaction

species	$\Delta_f H^0_{298}$/kJ mol^{-1}	species	$\Delta_f H^0_{298}$/kJ mol^{-1}
CH_3CHCH_2	20.4[a] [18]	cyclo-C_3H_4	277.1 ± 2.5[20]
cyclo-C_3H_6	53.3 ± 0.6[21]	H	218.0 ± 0.006[19]
CH_4	−74.9 ± 0.3[19]	CH_3	145.7 ± 0.8[19]
C_2H_4	52.3[a] [18]	C_2H_3	300.0 ± 3.3[22]
C_2H_2	226.7 ± 0.8[19]	CH_2 $^3B_1$	388.7 ± 2.5[22]
CH_3CCH	184.9 ± 0.8[20]	CH_2C $^1A_1$	427.6 ± 16.7[22]
CH_2CCH_2	190.5 ± 1.2[20]	CH_2CHCH_2	173.2 ± 2.1[23]

[a] Uncertainties are not reported in the source.

The article is organized as follows. Section I (current) is an introduction. The ab initio quantum chemical study of the potential energy surface of reaction 1 is presented in section II, where major reaction channels are identified and conclusions regarding the mechanism of the reaction are reached. Section III describes the master equation-based modeling of the chemically activated route of reaction 1 (channels 1a and 1b), including the use of the microcanonical variational approach to the selection of the transition state and analysis of the rate constants and channel branching fractions of reactions 2 and 3. Discussions of the methods used, results, and comparison with other studies, where applicable, are, generally, inseparable from the descriptions of the topics discussed and thus are given throughout the text rather than in a separate section. Finally, a summary of the results is provided in section IV.

II. Analysis of the Potential Energy Surface of Reaction 1. Reaction Mechanism and Product Channels

The reaction between vinyl and methyl radicals has a large number of thermodynamically allowed product channels

$$C_2H_3 + CH_3 \rightarrow CH_3CHCH_2 \quad \Delta H^0_{298} = -425 \text{ kJ mol}^{-1} \quad (1a)$$

$$\rightarrow CH_2CHCH_2 + H \quad \Delta H^0_{298} = -54 \text{ kJ mol}^{-1} \quad (1b)$$

$$\rightarrow C_2H_2 + CH_4 \quad \Delta H^0_{298} = -294 \text{ kJ mol}^{-1} \quad (1c)$$

$$\rightarrow C_3H_6(\text{cyclopropane}) \quad \Delta H^0_{298} = -392 \text{ kJ mol}^{-1} \quad (1d)$$

$$\rightarrow CH_3CCH + H_2 \quad \Delta H^0_{298} = -261 \text{ kJ mol}^{-1} \quad (1e)$$

$$\rightarrow CH_2CCH_2 + H_2 \quad \Delta H^0_{298} = -255 \text{ kJ mol}^{-1} \quad (1f)$$

$$\rightarrow C_3H_4(\text{cyclopropene}) + H_2 \quad \Delta H^0_{298} = -169 \text{ kJ mol}^{-1} \quad (1g)$$

$$\rightarrow C_2H_4 + {}^3CH_2 \quad \Delta H^0_{298} = -5 \text{ kJ mol}^{-1} \quad (1h)$$

Experimental thermochemical data on the reactants and products of these channels are provided in Table 1.

Reactions 1a, 1b, and 1c have been experimentally observed and confirmed to be the primary product channels of the $C_2H_3 + CH_3$ reaction.[7−9] It was suggested on the basis of the experimental results that reaction 1c occurs via a direct abstraction of a hydrogen atom from the vinyl radical by methyl radical whereas the products of channel 1b are formed as a result of the decomposition of a chemically activated adduct (CH_3CHCH_2), which can also undergo collisional stabilization (reaction 1a).

Isomerization to cyclopropane (reaction 1d) and the elimination of H_2 with the formation of propyne, allene or cyclopropene (reactions 1e, 1f, or 1g, respectively) are the alternative pathways of rearrangement of the chemically activated adduct. Cyclopropane could not be distinguished from propene in our experimental work[7] but it was detected in the product analysis work of Fahr et al.[9] at low levels (∼2−5%). As follows from the modeling performed by Fahr et al.[9] and Thorn et al.,[8] as well as from the reaction model created in the current study, isomerization of the vibrationally excited propene to cyclopropane and the corresponding reverse reaction are processes that occur in the system of the $C_2H_3 + CH_3$ reaction but have minor importance.

In our experimental study[7] of reaction 1, C_3H_4 isomers (the products of potential reaction channels 1e, 1f, and 1g) were searched for but could not be detected. C_3H_4 was formed in the experiments of Thorn et al.[8] but was suggested by the authors to be a product of secondary reactions. Reaction channels 1e, 1f, and 1 g, although not observed in experiments, cannot be ruled out completely. It may still be possible that these potential product channels have branching fractions that are small (below the experimental detection level) under the experimental conditions used but larger under other conditions.

Reaction channel 1h can be ruled out on the basis of the high energy barrier. Böhland et al.[24] have estimated the barrier of the reverse reaction (abstraction of an H atom from C_2H_4 by $^3CH_2$) using the Evans−Polanyi correlation to be 50 kJ mol^{-1}. Thus, the estimate of the barrier for the direct reaction 1h is ∼45 kJ mol^{-1}, which, considering the competition with barrierless addition and barrierless (or almost barrierless, see below) disproportionation (1c), makes the contribution of channel 1h negligible. This conclusion is in good agreement with the experimental results because no C_2H_4 product was detected within the range of experimental conditions used.[7]

The quantum chemical study of the potential energy surface (PES) of reaction 1 performed in the current work has dual purpose. One of its goals is to analyze the mechanism of reaction 1: confirm or refute the chemically activated routes of channels 1a and 1b; examine the feasibility of channels 1e, 1f, and 1 g; examine the possibility of formation of channel 1c products in the chemically activated route of reaction 1; and analyze the PES of the disproportionation reaction channel 1c. The second goal is to provide information on the reaction 1 PES that is needed to build the RRKM/master equation model. Because the quantum chemical study has a relatively subservient role in the current work, this section presents only its conclusions pertaining to the mechanism of the reaction between C_2H_3 and CH_3. A detailed description of the PES study is presented in the Supporting Information. In addition, a study of the properties of the reaction paths of propene decomposition leading to $C_2H_3 + CH_3$ and to $H + C_3H_5$ products is described in section III, along with the RRKM/master equation model, with details presented in the Supplement.

PES and the Mechanism of the C_2H_3+CH_3 Reaction. Two main computational approaches were employed in this study: Gaussian 2 (G2)[25] and QCISD(T)/6-311+G(2df,2p)//B3PW91/6-31G(d,p).[26−28] These two methods were chosen to provide similar high accuracy together with reasonable computational

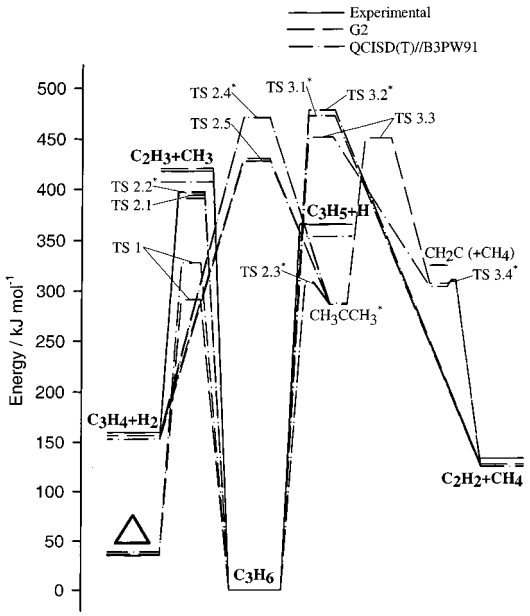

Figure 1. Potential energy diagram of the $C_2H_3 + CH_3$ reaction. For species marked with asterisk, G2, and QCISD(T)//B3PW91 energies coincide on the diagram. A detailed description of the PES study is presented in the Supporting Information.

speed. Each of them was used for each structure on the potential energy surface under study in order to assess the reliability of the results. Intrinsic reaction coordinate (IRC)[29] calculations in mass-weighted internal coordinates[30] were performed for each optimized saddle point structure in order to verify the connected reactants and products. All of the calculations were carried out using the Gaussian 98[31] and Gaussian 94[32] packages of programs.

The results of the quantum chemical study of the potential energy surface of reaction 1 can be summarized in the form of a mechanism that differs very little from the one suggested on the basis of experimental results.[7−9] The PES diagram is presented in Figure 1 and the calculated values of energies are given in Table 2. The reaction mechanism consists of two processes: radical addition followed by rearrangements and decomposition of the vibrationally excited adduct, and abstraction of an H atom from C_2H_3 by the methyl radical. The major route of further reaction of the chemically excited adduct (C_3H_6, propene) is its decomposition into an H atom and allyl radical. Isomerization to cyclopropane is an important reversible process. Because the microscopic energy-dependent rates of the reverse isomerization of cyclopropane to propene are larger than those of the direct reaction (due to the higher enthalpy of formation of cyclopropane compared to propene),[8,9] isomerization back to propene is expected to be fast and the fraction of cyclopropane among the final reaction products can be expected to be minor. H_2 elimination reactions do not play any role in the chemically activated propene decomposition in the $C_2H_3 + CH_3$ system.

The formation of acetylene and methane does not occur via the decomposition of the chemically activated propene, as follows from the large values of energy barriers for such routes. These products are formed in the abstraction (disproportionation) reaction which may proceed in two different ways. The first possibility is a reaction through a shallow-well, loosely bound intermediate complex followed by a transition state, the energy of which is below or slightly above the energy of the reactants. Alternatively, the reaction can be a simple barrierless process that does not involve any intermediates or saddle points. The results of the quantum chemical study of the PES are not conclusive regarding the choice between these two patterns. Both can explain the experimentally observed negative temperature dependence of the rate constant of formation of C_2H_2 and CH_4.[7] A similar formation of an intermediate complex in a hydrogen abstraction reaction has been suggested earlier by Russell and co-workers in order to explain the negative temperature dependences of the rate constants of the reactions of HBr with CH_3, C_2H_5, *i*-C_3H_7, and *t*-C_4H_9 radicals.[33−35] Their hypothesis was later corroborated by quantum chemical calculations and RRKM analysis carried out by Chen and co-workers for the H-atom abstraction from the hydrogen halides by methyl and ethyl radicals.[36−38] Recently, Peng et al.[39] and Krasnoperov et al.[40] confirmed the same qualitative shapes (loosely bound intermediate → energy barrier) of the potential energy profiles in the H-atom abstraction reactions of CH_3 and C_2H_5 radicals with HBr.

TABLE 2: Energies of Reactants, Products, Intermediates, and Transitions States of the $C_2H_3 + CH_3$ Reaction (relative to propene, kJ mol^{-1})

species	G2 ΔE^a	QCISD(T)//B3PW91 ΔE^b	expt $\Delta H°$ (0 K)^c
$C_2H_3 + CH_3$	420.5	407.3	418
CH_3CHCH_2	0.0	0.0	0.0
$CH_2CHCH_2 + H$	365.4	353.5	365
cyclo-C_3H_6[d]	36.6	39.1	35
$CH_3CCH + H_2$	156.4	152.9	160
$C_2H_2 + CH_4$	127.3	125.0	133
$CH_2C (+ CH_4)$	307.0	303.6	325
CH_3CCH_3	286.1	287.5	
TS 1	291.2	327.7	
TS 2.1	394.0	391.0	
TS 2.2	397.6	396.4	
TS 2.3	307.4	308.4	
TS 2.4	470.9	470.7	
TS 2.5	430.3	427.6	
TS 3.1	472.3	472.5	
TS 3.2	478.0	478.0	
TS 3.3	450.4	451.4	
TS 3.4 (+ CH_4)	308.8	310.6	

[a] Energy relative to CH_3CHCH_2 calculated at the G2 level of theory. Zero-point vibrational energies are included. [b] Energy relative to CH_3CHCH_2) calculated at the QCISD(T)/6-311+G(2df,2p)//B3PW91/6-31G(d,p) level of theory. Zero-point vibrational energies are included. [c] $\Delta H° = \Delta_f H^0_0$ (species) − $\Delta_f H^0_0(CH_3CHCH_2)$ calculated using experimental thermodynamic data (Table 1). [d] Cyclopropane.

The results of this study provide mechanistic information for another important process, the thermal decomposition of propene. Analysis of the potential energy diagram in Figure 1 indicates that the following reactions are potentially important in the thermal decomposition reaction

$$CH_3CHCH_2 \rightarrow H + CH_2CHCH_2$$
$$\rightleftarrows \text{cyclo-}C_3H_6$$
$$\rightarrow C_2H_3 + CH_3$$

The most thermodynamically favorable channel of rearrangement of cyclopropane (in addition to the reverse isomerization to propene) is the decomposition reaction[24]

$$\text{cyclo-}C_3H_6 \rightarrow C_2H_4 + {}^1CH_2 \quad \Delta H^0_0 = 416 \text{ kJ mol}^{-1}$$

The potential energy of the products of this reaction is 140 kJ mol^{-1} higher than the energy of the isomerization barrier (transition state TS1). Therefore, formation of cyclopropane can function only as a temporary sink of the C_3H_6 species.

III. Model of the Chemically Activated Route of the $C_2H_3 + CH_3$ Reaction

The mechanism of reaction 1 consists of two major routes: a direct hydrogen atom abstraction from C_2H_3 by the methyl radical (disproportionation) and the formation of chemically activated propene, which can stabilize, rearrange to cyclopropane, or decompose to an H atom and allyl radical. Modeling of the disproportionation route (channel 1c) would bear little meaning because of the large uncertainties associated with the properties of the potential energy surface (Section II). This reaction route rate constant, however, is not expected to depend on pressure and thus is a function of temperature only. Experimental values of the channels 1c rate constants have been obtained[7] in the 300−900 K range and can be represented with the expression

$$k_{1c} = 1.5 \times 10^{-11} \exp(385\ \mathrm{K}/T)\mathrm{cm}^3\ \mathrm{molecule}^{-1}\ \mathrm{s}^{-1}$$

In contrast to those of the abstraction route, the rate constants of the chemically activated route of the reaction and the resulting product channels are both pressure and temperature dependent. Computational modeling based on theories of unimolecular reactions must be used to provide extrapolation of the experimental data[7] to other temperatures and pressures. This section describes the RRKM/master equation analysis of the chemically activated route of reaction 1. The model was created using the results of the quantum chemical calculations and the experimental data.

III.1. General Computational Method. The mechanism of the chemically activated route of reaction 1 consists of the following processes

$$\text{(A) } C_2H_3 + CH_3 \rightleftarrows CH_2CHCH_3(E,J) \quad k_A(E,J),\ k_{-A}(E,J)$$

$$\text{(D) } CH_2CHCH_3(E,J) \rightarrow H + CH_2CHCH_2 \quad k_D(E,J) \qquad \text{(II)}$$

$$\text{(I) } CH_2CHCH_3(E,J) \rightleftarrows \text{cyclo-}C_3H_6(E,J) \quad k_I(E,J),\ k_{-I}(E,J)$$

$$\text{(ET) } CH_2CHCH_3(E,J) \rightarrow CH_2CHCH_3(E',J') \quad \omega P(E',J';E,J)$$

Here, $CH_2CHCH_3(E,J)$ means propene excited to energy E in the active[11−14] degrees of freedom with the quantum number of the total angular momentum J. On the right-hand side of Scheme II are listed the rate constants of these and the reverse (where applicable) processes. The $\omega P(E',J';E,J)$ "rate constant" is a product of the collision frequency with the bath gas ω and the probability of transition from energy E to energy E' and from angular momentum J to J' upon collision, $P(E',J';E,J)$. Indices A, D, I, and ET (left side of Scheme II) stand for "association," "decomposition," "isomerization," and "energy transfer," respectively.

The evolution of this type of system can be described by a two-dimensional (in E and J) master equation.[11,13] The solution of such a two-dimensional master equation is not only computationally intensive and cumbersome, but also meaningless unless a physically realistic model of the collisional energy transfer in rotational degrees of freedom is used. Given the current absence of reliable knowledge of the general properties of rotational energy transfer in collisions of bath gas with highly vibrationally excited polyatomic molecules, we prefer to reduce the two-dimensional problem to a one-dimensional one, in energy only.

In the reduced formulation, rotational effects are still taken into account in computation of the microcanonical rate constants $k(E,J)$ for reaction (−A). However, these $k(E,J)$ values are then averaged over the Boltzmann rotational distributions to provide temperature-specific energy dependent $k(E)$ functions (see subsection III.3 for details). Such treatment is equivalent to an assumption of very fast rotational equilibration. For reactive processes D and I, rotational effects can be expected to be minor (see below), and thus, only the J-independent k(E) values of the rate constants were calculated. Details of the master equation formulation are given in the Supporting Information.

Microcanonical rate constants $k(E,J)$ and $k(E)$ were computed using the RRKM method in combination with variational selection of the transition state. The variational approach requires information on the properties of the potential energy surface (PES) along the reaction paths. The next subsection (III.2) presents the quantum chemical computational study of these PES properties and subsection III.3 describes the calculation of the $k(E,J)$ functions.

III.2. Analysis of the Reaction Paths of Propene Decomposition. The B3PW91/6-31G(d,p) density functional method was selected for use in geometry optimization and calculation of projected frequencies[42,43] along the reaction paths of decomposition of propene. The choice of the computational method was based on the higher reliability of the structures and frequencies produced by density functional methods on spin-contaminated potential energy surfaces.[44] Intrinsic reaction coordinate[29] (IRC) calculations in mass-weighted internal coordinates[30] were performed in order to obtain structures located along the reaction paths. The IRC calculations were carried out in the "downhill" mode starting from the optimized structure obtained with a fixed, large separation of the departing fragments. QCISD(T)/6-311G(d,p) energies were obtained for the B3PW91-level IRC structures in order to refine the potential energy profiles along the reaction paths. In order for the potential energy profile to conform to the experimental reaction thermochemistry, the QCISD(T) energies were scaled with the ratio of the relative experimental energy of the products (with respect to propene, ZPE not included) to that obtained in the QCISD(T) calculations. The scaled QCISD(T) energies were interpolated with a polynomial function.

For each reaction channel, the projected vibrational modes were subdivided into two categories: transitional and nontransitional. The transitional modes correspond to the relative "rocking" motion of the separating fragments and evolve into rotational degrees of freedom at the products end of the reaction path. One transitional mode, that of the one-dimensional relative torsional rotation of the $-C_2H_3$ and $-CH_3$ fragments, has very low frequencies (5−90 cm^{-1} within the considered 2.3−3.8 Å range of the reaction coordinate) and, therefore, was approximated by a free internal rotor for the purpose of calculation of the microcanonical rate constants. The nontransitional modes converge to the normal modes of the products as the distance between the departing fragments increases. The dependences of the vibrational frequencies on the reaction coordinate were fitted with a polynomial function. The coefficients of the polynomial representation of each nontransitional mode were scaled with the ratio of the experimental to calculated frequencies of the corresponding vibrational mode of the products. The scaling procedure was performed in order to reduce errors in the calculated frequencies and to ensure that the calculated potential energy along the reaction paths, with ZPE included, converges to the experimental energy of the products in the limit of infinite separation of the fragments. The experimental frequencies of the products, rather than those of the reactants, were used in the scaling procedure because it was anticipated

that the transition states selected by the variational approach will be closer to products (in terms of structure). Rotational constants of the structures located along the reaction paths were also interpolated with a polynomial function. Details of the procedures and results are given in the Supporting Information.

III.3. Microcanonical Rate Constants. *Variational Selection of the Transition State and Calculation of k(E,J).* Microcanonical rate constants for reactions −A and D in Scheme II were calculated by the RRKM method.[11−14] Overall rotations of these molecules were approximated by a symmetric top model. For each species, one-dimensional overall rotation about the principal axis with the lowest moment of inertia was assumed to be active,[11−14] and the remaining two-dimensional overall rotation was considered inactive, or adiabatic. The overall angular momentum is approximated by that of the adiabatic rotor and is conserved during the course of the reaction.

The density-of-state and sum-of-states functions necessary for the calculation of microcanonical rate constants were computed using the modified Beyer−Swinehart algorithm.[45,46] The energy scale was divided into an array of bins of 50−100 cm^{-1} size. The densities and sums of states were computed with 10× smaller energy step sizes and then averaged for each energy bin. The density of states of the hindered internal rotor of propene was included in the overall density of states of the molecule using the method of Knyazev.[47]

The microcanonical rate constants of the decomposition of propene to $C_2H_3 + CH_3$ were calculated using a variational approach.[11−13] For each energy E and angular momentum quantum number J, the value of $k_{-A}(E,J)$ was minimized by varying the position of the transition state along the reaction coordinate. The minimization was performed by a grid search with a step size of 0.008 Å within the 2.3−3.8 Å range of the reaction coordinate. The scaled QCISD(T)/6-311G(d,p)//B3PW91/6-31G(d,p) energy profile of the reaction path together with the calculated dependences of frequencies and rotational constants on the reaction coordinate (subsection III.2) was used for the computation of the sums of states of the transition structures. At each point along the reaction coordinate, zero-point vibrational energy (ZPE, calculated using the scaled projected frequencies) was included in the potential energy profile.

The $k_{-A}(E,J)$ values obtained were averaged over the Boltzmann rotational distribution of propene for each temperature of interest. As a result, the energy- and J-specific rate constants are converted to the energy- and temperature-dependent ones. This J-averaging reduces the two-dimensional problem (in E and J) of competition between the reactions and the collisional energy transfer to a one-dimensional formulation (section III.1) which can be solved by existing methods. Details of calculations and relevant formulas are given in the Supporting Information.

In the case of decomposition of propene to $H + C_3H_5$ (reaction D in Scheme II), the rotational constant of the 2-dimensional inactive overall rotation changes by less than 10% along the reaction path within the 1.9−3.15 range of the reaction coordinate. Considering this insignificant dependence of the rotational constant on the reaction coordinate, the conservation of angular momentum for this reaction was taken into account approximately using the method originally introduced by Marcus[48] where the energy-dependent rate constants are corrected by the ratio of moments of inertia (or rotational constants) of the 2-dimensional adiabatic rotations of the transition state and the active molecule

$$k(E) = \frac{B\, W^{\neq}(E)}{B^{\neq} h\rho(E)} \qquad \text{(III)}$$

The energy-specific rate constants $k(E)$ were calculated using variational approach. At each energy E, a grid search with a step size of 0.007 Å was performed within the 1.9−3.15 Å range of the reaction coordinate to locate the position of the transition state on the reaction path corresponding to the minimum of $k_D(E)$. The scaled QCISD(T)/6-311G(d,p)//B3PW91/6-31G(d,p) energy profile of the reaction path (with ZPE included) together with the calculated dependences of frequencies and rotational constants on the reaction coordinate (subsection III.2) was used for the computation of the sums of states of the transition structures.

The microcanonical rate constants of the propene isomerization to cyclopropane (reaction I in Scheme 2) were calculated using RRKM theory and the vibrator-rotor approximation. The position of the transition state was fixed at the top of the energy barrier. Conservation of angular momentum was included via expression III. The B3PW91/6-31G(d,p)-level frequencies and rotational constants of the isomerization transition state were used in these calculations. The value of the isomerization energy barrier, as well as those of the four lowest vibrational frequencies, were adjusted to be consistent with the high-pressure-limit rate constant temperature dependence recommended by Furue and Pacey[49] and with the experimental thermochemical data (Table 1, also see section II).

All microcanonical rate constants were multiplied by the corresponding reaction path degeneracy values obtained from the ratios of rotational symmetry factors and numbers of optical isomers following the method described by Pechukas[50] and Karas et al.[51] (also see ref 11). Here, the existence of two optical isomers in the transition states for the propene isomerization to cyclopropene and for its decomposition to H and C_3H_5 was taken into account.

High-Pressure-Limit Rate Constants and Adjustment of the Model Parameters. The quantum chemical methods employed in this work cannot be expected to exactly describe all properties of the transition states involved in the complex mechanism of reaction 1. Thus, the least reliable parameters of the transition structures were adjusted to reproduce experimental kinetic data available for the high-pressure-limit rate constants of individual reaction channels. For the barrierless decomposition channels (reactions −A and D in Scheme II), the calculated dependences of the transitional frequencies on the reaction coordinate were multiplied by scaling factors, the latter being used as fitting parameters. Fitting was performed by minimizing the sum of the absolute values of the differences between the experimental and calculated rate constants. For the propene−cyclopropane isomerization, the reaction barrier and the four lowest frequencies of the transition state were adjusted.

The scaling factor for the four transitional frequencies of propene decomposition to $C_2H_3 + CH_3$ was adjusted (final value 0.49) to reproduce the experimental rate constants of the $C_2H_3 + CH_3$ combination reaction at 310 and 500 K obtained in our earlier experimental work.[7] It was assumed and later confirmed by master equation modeling that the addition step in reaction 1 is very close to its high-pressure limit ($k/k^{\infty} > 0.94$) at these temperatures and the experimental bath gas densities used, [He] = (3−12) × 10^{16} atoms cm^{-3}. The high-pressure-limit rate constants of reaction channel −A (k_{-A}^{∞}) were calculated by numerical integration of the microcanonical rate constants over the Boltzmann distribution of propene

$$k_{-A}^{\infty}(T) = \int_0^{\infty} k_{-A}(E, T) f_p(E, T) dE \qquad \text{(IV)}$$

where f_p is the normalized Boltzmann distribution in the active degrees of freedom of the propene molecule.

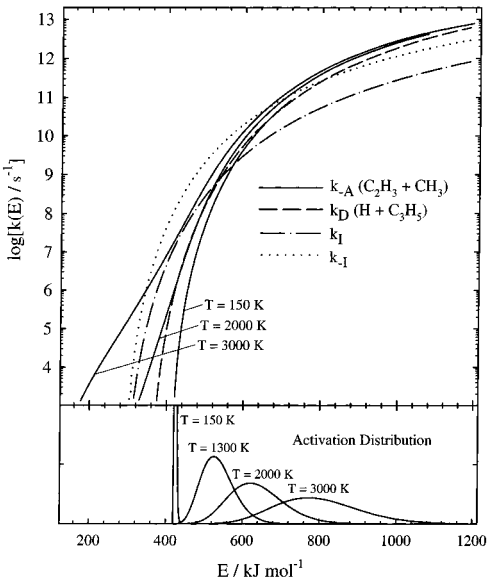

Figure 2. Energy dependences of the microcanonical rate constants of the decomposition and isomerization of C_3H_6. Upper graph: $k(E)$ values. Solid lines, the $C_3H_6 \rightarrow C_2H_3 + CH_3$ channel (J-averaged $k_{-A}(E)$ at three different temperatures); dashed line, the $C_3H_6 \rightarrow H + C_3H_5$ channel ($k_D(E)$); dashed-and-dotted line, the $C_3H_6 \rightarrow$ cyclo-C_3H_6 channel ($k_I(E)$); dotted line, the cyclo-$C_3H_6 \rightarrow C_3H_6$ channel (the reverse isomerization, $k_I(E)$). Lower graph: chemical activation distributions at different temperatures. All energies are relative to the zero-point vibrational energy of propene.

The scaling factor for the reaction channel of propene decomposition to H atom and allyl radical was adjusted to reproduce the high-pressure-limit rate constant of the $H + C_3H_5$ reaction reported by Hanning−Lee and Pilling[52] at 291 K and 13−53 kPa (98−400 Torr) of He ($k_{-D}^{\infty} = (2.8 \pm 1.0) \times 10^{-10}$ cm^3 molecule^{-1} s^{-1}). The rate constant value of the $C_3H_5 + H$ reaction reported in ref 52 has a substantial uncertainty. While the authors report 36% (2σ) uncertainty of the final rate constant value, individual rate constants obtained from the sets of measurements performed at different pressures differ by as much as a factor of 2.7 (with no clear pressure dependence). In the current model, the scaling factors of the transitional frequencies of the reaction channel D (Scheme II) were allowed to vary in such a way that the calculated high-pressure-limit rate constant of the $C_3H_5 + H$ reaction varied within the reported uncertainty of the experimental value. This additional degree of flexibility in the model properties was used in the master equation analysis of the experimental data on the product distribution in the $C_2H_3 + CH_3$ reaction (subsection III.4).

The energy dependences of the microcanonical rate constants of all the considered unimolecular channels of the $C_2H_3 + CH_3$ system are shown in Figure 2. As can be seen from the plot, the shape of the $k_{-A}(E,T)$ energy dependence displays a noticeable dependence on temperature, which is especially pronounced at low energies. The values of this microcanonical rate constant increase with the temperature due to the centrifugal decrease in the effective reaction barrier. Details of the model are given in the Supporting Information, where a discussion of the applicability of the harmonic approximation to the transitional modes is also presented.

III.4. Master Equation Modeling. *Methods of the Master Equation Solution.* The exponential-down model[11,13,53] was employed to describe the collisional energy transfer. The values of $\langle \Delta E \rangle_{down}$, the average energy transferred per "downward" collision, (assumed here to be equal for propene and cyclopropane) are unknown and thus were used as fitting parameters to reproduce the experimental data[7] on the kinetics and product distribution in the $C_2H_3 + CH_3$ reaction. For the purpose of solution of the time-dependent master equation (subsection III.1 and Supporting Information) it is converted into a discrete form (the energy scale is divided into an array of bins) so that equations can be expressed in terms of finite matrixes. The general matrix form of the master equation for unimolecular reactions can be found, for example, in refs 11,13 and the specific case of reactions including isomerization and decomposition is described by Bedanov et al.[15] Householder's algorithm[54] (tridiagonalization) and subsequently the implicit QR algorithm[54] (final diagonalization) were used to solve the equation in the matrix format. A detailed formulation of the solution of a similar type of discrete master equation is described in ref 15. An energy bin size of 50 cm^{-1} was used for all computations performed for temperatures below 1000 K; a 100 cm^{-1} energy bin size was used for temperatures above 1000 K. The sizes and the numbers of the energy bins used in the calculations were chosen in such a way that a 1.5× increase in the number of the bins or a decrease in the size of the bin by a factor of 2 produced less than a 5% difference in the final values of the computed rate constants and branching ratios. The Chemrate program[55] was employed to solve the master equation.

The solution of the master equation yields the eigenvalues and eigenvectors of the corresponding matrix[11,13,55] and the resultant energy- and time-dependent populations of propene ($g_p(E,t)$) and cyclopropane ($g_c(E,t)$). To obtain information on the overall rate constants and branching channel ratios of the $C_2H_3 + CH_3$ combination reaction, two approaches (implemented in the Chemrate program) were used.

In the first approach, the populations of propene and cyclopropane were divided into two parts: active and stabilized. The part of the population of each of these species located above the lowest-energy channel barrier (isomerization) was considered to be active and the part of the population located below this barrier was considered to be stabilized. The concentrations of vinyl and methyl radicals were set to be constant in the master equation. The rates of decomposition reaction channels (−A and D in Scheme II) were calculated by numerical integration of the corresponding microcanonical rate constants over the active population of propene. The rate of formation of propene was taken as equal to the rate of growth of the stabilized part of its population. The rate of propene isomerization to cyclopropane was taken to be equal to the rate of growth of the total population of cyclopropane.

From these rates, the branching ratios of channels 1a, 1b, and 1d were calculated. The rate constant of the overall $C_2H_3 + CH_3$ combination reaction was obtained as

$$k_{C_2H_3+CH_3} = k_A^{\infty}(1 - r_{-A}) \qquad \text{(V)}$$

where k_A^{∞} is the high-pressure-limit rate constant of the reaction channel A (Scheme II) and r_{-A} is the fraction of propene molecules that decompose back to C_2H_3 and CH_3.

The calculation of the branching channel ratios was performed at times when the active parts of the time-dependent populations of propene and cyclopropane reached their corresponding steady-states and, as a result, the computed rates of channels 1a, 1b, and 1d did not change with time. This approach gives correct results under the conditions where the rate constants of thermal decomposition and isomerization of propene and cyclopropane are negligibly small. Under these conditions, the stabilized (thermal) and active part of the populations are well-separated from each other on the energy scale and the accumulation of

the stabilized propene and cyclopropane does not affect the active parts of their populations. At high temperatures, however, the accumulation of the stabilized products does affect the energy distributions in the parts of the populations located above the isomerization barrier (i.e., thermal reactions of the stabilized species have nonnegligible rates). As a result, the steady state of the active parts of the populations is not reached until the whole system reaches dynamic equilibrium, i.e., the rate of decomposition of the stabilized species is equal to the rate of their formation. The description of the qualitative behavior of chemically activated systems and the discussion of the relative roles of the two steady states can be found, for example, in refs 56−59.

This type of behavior where thermal processes interfere with the chemically activated kinetics was observed in the $C_2H_3 + CH_3$ system starting from temperatures as low as 900 K. At 900 K, however, only the rates of stabilization (channel 1a) and isomerization (channel 1d) were affected. The sum of the rates of channels 1a and 1d did not change with time (after a short induction period, $<10^{-5}$ s), so that the approach described above could still be used to determine the branching ratio of the overall stabilization.

For temperatures above 900 K, the *virtual component* formalism[16] of Knyazev and Tsang had to be employed to describe the system in terms of time-independent rate constants. This formalism was developed to enable the interpretation in terms of time-independent rate constants of the general case of unimolecular kinetics (including non-steady-state behavior,[16,56,60−64] when the rates of reactions change in time together with the rapidly evolving energy distributions). Such interpretation enables the incorporation of non-steady-state kinetics into large reaction schemes, such as those used to model the chemistry of combustion. As a limiting, simplest specific case of the general solution, the *virtual components* formalism provides the steady-state rate constants of chemically or photochemically activated unimolecular reactions. The detailed formulation of this approach can be found in ref 16 and only a brief conceptual description is given below.

The population of propene is presented as a combination of "virtual components" due to eigenvectors of the master equation matrix. The number of the virtual components is equal to the size of the master equation matrix (the number of the energy bins). Under any condition, the temporal behavior of the reactive system can be described in terms of the time-independent rate constants of the formation and decomposition of these virtual components. For all conditions used in this work, the rate constants of decomposition of the virtual components are orders of magnitude higher than the rate of the overall process with the exception of the one rate constant which corresponds to the lowest (in absolute value) eigenvalue of the master equation matrix. The steady-state of the part of the propene population described by these virtual components is reached instantaneously on the time scale of the overall reaction. Thus, their contribution does not need to be considered explicitly and can be described[16] as a pseudo-direct reaction leading from the $C_2H_3 + CH_3$ reactants to the $C_3H_5 + H$ products. The virtual component corresponding to the remaining lowest eigenvalue of the master equation matrix (referred to as "the thermal component" below) has an energy distribution which is equivalent to the distribution of thermally decomposing propene under the same conditions. Accordingly, the rate constant of decomposition of the thermal virtual component is equal to the rate constant of thermal decomposition of propene under the same conditions.

Within the *virtual component* formalism, the kinetics of the chemically activated route of the $C_2H_3 + CH_3$ reaction can be described in terms of time-independent rate constants using the following kinetic scheme

$$\begin{aligned} &C_2H_3 + CH_3 \rightarrow H + C_3H_5 && \text{(1b)}\\ &C_2H_3 + CH_3 \rightarrow C_3H_6\ \text{(thermal)} && \text{(1a)}\\ &C_3H_6\ \text{(thermal)} \rightarrow C_2H_3 + CH_3 && \text{(2a)}\\ &C_3H_6\ \text{(thermal)} \rightarrow H + C_3H_5 && \text{(2b)} \end{aligned} \qquad \text{(VI)}$$

Here, channel 1b is the pseudo-direct reaction that accounts for the contribution of all the virtual components except for the thermal one. C_3H_6 (thermal) represents stabilized propene described by the thermal virtual component. The rate constants of formation of allyl radical and H-atom (channel 1b), formation of propene (stabilization, channel 1a), and thermal decomposition of propene (channels 2a and 2b) are obtained via the formulas in ref 16. Reaction 2a appears to be the reverse of reaction channel 1a. However, because an equilibrium constant, in general, cannot be used here to relate their respective rate constants, a different reaction numbering is used to avoid potential confusion.

The isomerization of propene to cyclopropane is not included in the above reaction Scheme VI because the *virtual component* formalism for chemical activation systems which include reversible isomerization has not yet been developed. Fortunately, for the system of reaction 1, this isomerization channel is minor under all conditions. Although the microcanonical rate constants of the propene isomerization to cyclopropane (reaction I in Scheme II) dominate at low energies over the $k(E)$ of the other propene reaction channels (those of propene decomposition, see Figure 2), the rate constants of the reverse process, isomerization of cyclopropane to propene, are even larger. Calculations were performed to demonstrate that, for the purpose of the application of the virtual component formalism, the isomerization channel can be excluded from the kinetic scheme of the $C_2H_3 + CH_3$ combination reaction without serious implications for the accuracy of the computed results (Details are described in the Supporting Information). The main effect of this exclusion is that the calculated rates of stabilized propene formation account for the formation of both propene and cyclopropene without distinguishing between these two isomers.

Analysis of Experimental Product Branching Data on the Chemically Activated Route of the $C_2H_3 + CH_3$ Reaction. The parameters of the model of the $C_2H_3 + CH_3$ combination reaction (the chemically activated route of reaction 1) were adjusted to reproduce the branching ratios of this reaction obtained in our recent experimental study[7] at temperatures of 310, 500, and 900 K, and bath gas (He) densities of 3×10^{16} and 12×10^{16} atoms cm^{-3}. The average energy transferred per deactivating collision, $\langle \Delta E \rangle_{down}$, was used as the main fitting parameter. All of other parameters of the model were fixed at the values derived from the experimental information (e.g., energetics of the reaction channels, frequencies of the reactants and products), quantum chemical calculations (e.g., potential energy profiles of the barrierless reactions, rotational constants) or obtained by fitting experimental data on the high-pressure-limit rate constants (scaling factors of transitional frequencies, the height of the barrier of isomerization of propene to cyclopropane).

Modeling is complicated by the unknown temperature dependence of $\langle \Delta E \rangle_{down}$ which had to be taken into account.

An assignment of a functional form to the temperature dependence of the properties of collisional energy transfer is necessary for extrapolation of the experimental results beyond the experimental temperature range. Three different models of the temperature dependence of $\langle\Delta E\rangle_{down}$ were tested for the fitting of the experimental data: $\langle\Delta E\rangle_{down}$ = constant (no temperature dependence), $\langle\Delta E\rangle_{down}$ proportional to T, and $\langle\Delta E\rangle_{all}$ = constant, where $\langle\Delta E\rangle_{all}$ is the average energy transferred per collision in both upward and downward directions.[11] The values of $\langle\Delta E\rangle_{all}$ that were used in calculations were calculated at the propene energy equal to that of the $C_2H_3 + CH_3$ reactants.

The dependence of collisional energy transfer parameters such as $\langle\Delta E\rangle_{down}$ on temperature is, generally, unknown and constitutes a subject of ongoing research by many groups. The $\langle\Delta E\rangle_{down}$ = constant model presents the simplest choice and, following the Occam's razor approach, is frequently used in modeling attempts. This independence of $\langle\Delta E\rangle_{down}$ of temperature is also supported by theoretical results of Borjesson and Nordholm[65,66] and Ming et al.[67] The proportional dependence was derived[68,69] from modeling of the experimental falloff data in the

$$H + C_2H_4 \rightleftarrows C_2H_5 \qquad (4)$$

reaction obtained at temperatures ranging from 298 to 1100 K. A similar proportional dependence was obtained by Knyazev and Tsang[59] in their modeling of the experimental data on the chemically and thermally activated decomposition of secondary butyl radical in the 195−680 K temperature range. The $\langle\Delta E\rangle_{all}$ = constant model represents an intermediate case of the $\langle\Delta E\rangle_{down}$ temperature dependence: $\langle\Delta E\rangle_{down}$ increases with temperature but more slowly than in the case of the directly proportional model. The use of the $\langle\Delta E\rangle_{all}$ = constant model for the description of collisional energy transfer phenomenon has been advocated by several research groups. The independence of $\langle\Delta E\rangle_{all}$ on temperature is supported by the results of both experimental and trajectory studies of collisional energy transfer in large polyatomic molecules.[70,71] This collisional energy transfer model has been successfully used to reproduce the results of experimental studies of the thermal decomposition reactions of small molecules.[72,73] Dashevskaya et al.[74] predict the $\langle\Delta E\rangle_{all}$ = constant dependence for He as a bath gas within the framework of the sequential direct encounter model.

Fitting of the experimental data was performed by minimizing the sum of absolute deviations (on a logarithmic scale) between the calculated and the experimental values of the stabilization-to-decomposition ratio. Experimental data obtained at 310 and 500 K were used. The experimental data at 900 K have significantly larger uncertainties and hence were not included in the optimization. The sum of the reaction channels 1a and 1d (propene and cyclopropane) was taken as the measure of stabilization in the calculations. It was found that, of the three models of the $\langle\Delta E\rangle_{down}$ vs T dependence considered, the best agreement between the experimental and calculated data was obtained with the $\langle\Delta E\rangle_{all}$ = constant model. A grid search with a step size of 20 cm^{-1} yielded the optimum values of $\langle\Delta E\rangle_{all}$.

In the calculation of the microcanonical $k_D(E)$ values for the channel of decomposition of propene to $H + C_3H_5$, the scaling factors of the transitional frequencies of that reaction channel were allowed to vary in such a way that the calculated high-pressure-limit rate constant of the $C_3H_5 + H$ addition reaction varied within the reported uncertainty of the experimental value,[52] $k_{-D}^{\infty}(291K) = (2.8 \pm 1.0) \times 10^{-10}$ cm^3 $molecule^{-1}$ s^{-1} (See subsection III.3.). This uncertainty of the k_{-D}^{∞} value results in an additional flexibility of the model of reaction 1. Modeling of the experimental channel branching data[7] performed with the "central" version of the model based on the central value of $k_{-D}^{\infty} = 2.8 \times 10^{-10}$ cm^3 $molecule^{-1}$ s^{-1} resulted in values of $\langle\Delta E\rangle_{all}$ that are unrealistically large: $\langle\Delta E\rangle_{all} = -810$ cm^{-1}, which corresponds to $\langle\Delta E\rangle_{down}$ equal to 1000 cm^{-1} at 310 K and 1320 cm^{-1} at 900 K. Reduction of the calculated rate constant of the $H + C_3H_5$ reaction to the lower limit of the experimental value ($k_{-D}^{\infty}(291K) = 1.8 \times 10^{-10}$ cm^3 $molecule^{-1}$ s^{-1}) results in the more realistic fitted value of $\langle\Delta E\rangle_{all} = -500$ cm^{-1}.

The effects of variations in $\langle\Delta E\rangle_{all}$ and in k_{-D}^{∞} on the results of the master equation modeling of the reaction 1 branching fractions are not independent. Both of these variations affect the competition between the decomposition (the efficiency of which is linked to the k_{-D}^{∞} value) and the stabilization (controlled by $\langle\Delta E\rangle_{all}$) of the chemically activated propene. Thus, for any reasonably chosen value of k_{-D}^{∞} it is possible to find a corresponding value of $\langle\Delta E\rangle_{all}$ that will reproduce the experimental data. We select for the purpose of further use the model of reaction 1 with the $H+C_3H_5$ "exit" channel parameters (transitional frequencies scaling coefficients) resulting from the use of the lower-limit value of $k_{-D}^{\infty}(291K) = 1.8 \times 10^{-10}$ cm^3 $molecule^{-1}$ s^{-1}. This selection is based purely on the more realistic value of $\langle\Delta E\rangle_{all} = -500$ cm^{-1} obtained from fitting of the experimental branching data on reaction 1 with this model.

As has been mentioned above, although the reported error limits of the experimental k_{-D}^{∞} value in ref 52 are only 36% (2σ), the individual rate constants obtained in different sets of measurements differ by as much as a factor of 2.7, which can be interpreted as a sign of larger uncertainty. This uncertainty propagates into that of the $\langle\Delta E\rangle_{all}$ values obtained in the current work. A lower rate constant of the $H + C_3H_5$ reaction would result in even lower fitted $\langle\Delta E\rangle_{all}$. For example, $k_{-D}^{\infty}(291K) = 1.0 \times 10^{-10}$ cm^3 $molecule^{-1}$ s^{-1} would reduce the optimal value of $\langle\Delta E\rangle_{all}$ to ~ -250 cm^{-1}.

The calculated values of the S/D stabilization-to-decomposition ratios are presented in Figure 3 (lower plot) together with the experimental values.[7] As can be seen from the plot, the model reproduces the experimental data with deviations comparable to the uncertainties of the experiments. The temperature dependence of the overall rate constant of the $C_2H_3 + CH_3$ combination reaction (the addition − chemical activation route) is presented in the upper plot in Figure 3. The experimental data are well reproduced by the calculations. Reaction 1 is very close to the high-pressure limit at 310 and 500 K and the experimental bath gas pressures (less than 6% of the activated propene decomposes back to vinyl and methyl radicals). At 900 K and the experimental bath gas concentrations, about 25% of the activated propene decomposes backward, as can be seen from comparison of the dotted line (the high-pressure-limit rate) with the solid and the dashed lines (rate constants at [He] = $(3.0-12) \times 10^{16}$ atoms cm^{-3}). The importance of the adduct (propene) reverse decomposition increases with temperature, as can be inferred from the dependences (k(E) and chemical activation distributions) presented in Figure 2. As can be seen from the plots, the J-averaged microcanonical rate constants of the reverse propene decomposition to $C_2H_3 + CH_3$ are larger than those of the "direct" decomposition to $H + C_3H_5$ at higher energies. As the temperature increases, the chemical activation distribution shifts to higher energies. Also, centrifugal effects increase with temperature resulting in larger microscopic rates for the reverse decomposition even at low energies. These two effects combined result in an increase in the relative importance of the reverse dissociation of the propene adduct with temper-

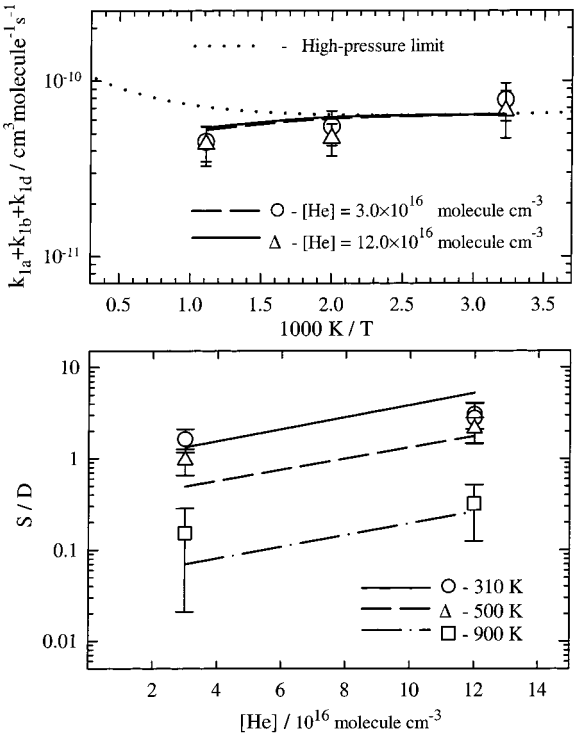

Figure 3. Experimental data (symbols) and calculated values (lines) of the overall rate constants of the combination (chemically activated) route in reaction 1 (channels 1a, 1b, and 1d combined) and stabilization-to-decomposition branching ratios. Upper graph: Arrhenius plot of $k(T) = k_{1a}(T) + k_{1b}(T) + k_{1d}(T)$. Lower plot: stabilization-to-decomposition ratios ($S/D = (k_{1a} + k_{1d})/k_{1b}$) as functions of the bath gas density at three experimental temperatures.

ature. A similar effect, the change in the channels branching fraction with temperature, is observed for the thermal decomposition of propene (see below).

Thermal Decomposition of Propene. The model of the $C_2H_3 + CH_3$ combination reaction created here incorporates, as a specific case, another important process, that of thermal decomposition of propene

$$CH_2CHCH_3 \rightarrow C_2H_3 + CH_3 \quad (2a)$$

$$\rightarrow H + C_3H_5 \quad (2b)$$

$$\rightleftarrows \text{cyclo-}C_3H_6 \quad (2c)$$

Experimental determination of the rate constants of reaction 2 is complicated due to the large number of fast secondary reactions which follow the initial dissociation step in the propene pyrolysis. Kiefer et al.[17] studied this pyrolysis process using the shock tube/laser-schlieren technique, which provides an accurate measure of the net rate of an endothermic reaction within 1 μs of shock heating, where the initial dissociation of propene (at high temperatures, >1500 K) should be the dominant process. The authors determined the overall rate constant of decomposition of propene over the temperature range 1650−2300 K and at bath gas concentrations of $(6-13) \times 10^{17}$ molecule cm^{-3}. Kr and propene (the reactant) were used (separately) as bath gases (M) in these experiments. No clear difference between the results obtained in the two bath gases was observed. The temperature dependences of the second-order overall rate constants obtained by Kiefer et al. are shown in Figure 4 (the upper graph). Both the rate constants obtained by a simple extrapolation of the density gradient to the zero of the time scale ("preliminary" results as reported in ref 17, dashed

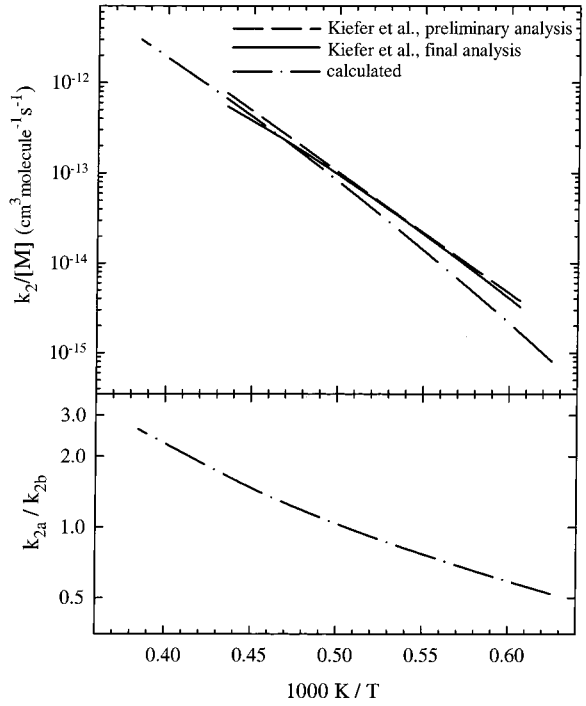

Figure 4. Experimental[17] and calculated data on the temperature dependence of the rate constant of thermal decomposition of propene (reaction 2). Upper graph: dashed line, the "preliminary" shock tube/laser schlieren results of Kiefer et al.[17] obtained by an extrapolation of the density gradient to the zero of the time scale; solid line, the "final" results of Kiefer et al. obtained via kinetic modeling of the reactive system used in the experiments; dashed-and-dotted line, the results of calculations performed in the current work. Lower graph: the ratio of the rate constants of reaction channels 1b and 1a obtained in the calculations (for the conditions of the experiments of Kiefer et al.[17]) as a function of temperature.

line) and those derived from a detailed simulation of the gradient behavior using a 23-step reaction mechanism of the pyrolysis process ("final" results, ref 17, solid line) are shown on the graph.

To model the decomposition/isomerization reaction 2, the master equation with the chemical activation term removed was solved as described above. Kr bath gas at a concentration of 9.5×10^{17} atoms cm^{-3} (median of the experimental concentration range of Kiefer et al.) was used in these calculations. All parameters of the model including $\langle \Delta E \rangle_{all}$ were set to the same values that were obtained in the modeling of the $C_2H_3 + CH_3$ combination reaction. The collisional energy transfer parameter for the Kr bath gas can differ from that for He. However, in the absence of knowledge of this parameter for Kr, the value of $\langle \Delta E \rangle_{all} = -500$ cm^{-1}, obtained for He bath gas in the modeling of the $C_2H_3 + CH_3$ system, was used. The rate constants of channels 2a and 2b were calculated by numerical averaging of the corresponding microcanonical rate constants over the distribution of propene obtained as a result of the solution of the master equation. The averaging was performed at times after the energy distribution of the propene molecules reached a steady-state (i.e., the shape of the distribution did not change with time). The results of the solution of the master equation demonstrate that thermal equilibrium between propene and cyclopropane is reached very quickly relative to the time scale of the decomposition reaction. The rate of isomerization of propene to cyclopropane (rate of channel 2c, calculated as the rate of accumulation of cyclopropane) is negligible for all sets of conditions considered.

The temperature dependence of the calculated overall rate constant of decomposition of propene is shown as a dash−dot line in the upper graph of Figure 4. The temperature dependence of the ratio of the calculated rate constants of channel 2a to channel 2b is presented in the lower graph. The model is in good agreement with the results of Kiefer and coauthors at higher temperatures but deviates from the experimental results at the lower end of the temperature range. At $T = 1650$ K, the calculated and the measured values of the overall rate constant differ by a factor of 2. The difference in the slope between the calculated and the experimental temperature dependences can be attributed either to the inadequacy of the collisional energy transfer model (which was successfully used for He but may not be valid for Kr) or to the shortcomings of the kinetic model used by the authors of ref 17. In the simulation of the gradient behavior performed to obtain the final values of the experimental rate constants, these authors assumed channel 2a to be the only channel of thermal decomposition of propene. However, according to the results of the current modeling, channel 2a indeed becomes the dominant channel of the decomposition reaction, but only at temperatures above 2000 K. At the lower end of the experimental temperature range, where the disagreement is observed between the calculated rates and those derived from the experimental data, the major decomposition channel is reaction 2b.

Prediction of the Rate Constants and Branching Fractions of the $C_2H_3 + CH_3$ Combination Reaction, Thermal Decomposition of Propene, and the $H + C_3H_5$ Reaction over Wide Ranges of Conditions. The overall rate constant and branching channel fractions of the $C_2H_3 + CH_3$ combination reaction (the chemically activated route, channels 1a, 1b, and 1d) were calculated within a broad range of pressures (0.1333−1333 kPa, or 1−10 000 Torr) and temperatures (150−3000 K). The calculations were performed for He bath gas using the parameters of the reaction model obtained in the fitting of the experimental data on the $C_2H_3 + CH_3$ reaction (see above). The results of these calculations are presented in Table 3. The temperature dependence of the high-pressure-limit rate constant and the pressure dependences of the overall reaction rate (at different temperatures) are shown in Figures3 and 5, respectively. Figure 5 also shows the pressure dependences of the stabilization-to-decomposition ratio ($S/D = (k_{1a} + k_{1d})/k_{1b}$) and the "intuitive"[41,59] rate of decomposition of the chemically activated propene, k_a

$$k_a = \omega\frac{D}{S} \qquad \text{(VII)}$$

According to the results of the calculations, the high-pressure-limit rate constant of the $C_2H_3 + CH_3$ combination reaction experiences a weak temperature dependence, decreasing slightly with increasing temperature within the 150−500 K temperature range and increasing with increasing temperature within the 500−3000 K temperature range (Figure 3). This dependence can be represented with the expression

$$k^{\infty}_{1a}(T) = 3.51 \times 10^{-12}\, T^{0.417} \exp(161\ \text{K/T})\ \text{cm}^3\ \text{molecule}^{-1}\ \text{s}^{-1} \qquad \text{(VIII)}$$

(The k^{∞}_{1a} notation is used here since only the stabilization channel is present in the high-pressure limit). In the low-pressure limit, the only channel of the chemically activated reaction route is the formation of H atom and allyl radical, channel 1b. The temperature dependence of the low-pressure-limit rate constant obtained in the modeling can be represented by the expression

$$k^{0}_{1b}(T) = 3.42 \times 10^{-10}\, T^{-0.285}\ \text{cm}^3\ \text{molecule}^{-1}\ \text{s}^{-1} \qquad \text{(IX)}$$

Between 150 and 500 K, the overall rate constant of the $C_2H_3 + CH_3$ combination reaction is in the high-pressure limit at pressures above 1 Torr and formation of propene is the dominant product channel above 10 Torr. For temperatures above 2400 K, the overall rate constant is in the low-pressure limit and the only products of the combination reaction are allyl radical and H-atom (with the exception of the highest pressure considered, 10 000 Torr, where some stabilization still occurs at 2400 K). In the intermediate temperature range, 500−2400 K, the overall rate constant and the branching fractions of the product channels of the $C_2H_3 + CH_3$ combination reaction exhibit both pressure and temperature dependence (Figure 5).

The pressure dependences of the stabilization-to-decomposition ratio are shown in the middle part of Figure 5. For those temperatures (150−900 K) where the calculations were performed with the channel of reversible isomerization of propene to cyclopropane included in the computational scheme, the contribution of the channel of formation of cyclopropane is included in the stabilization. The contribution of this channel is minor under all conditions: the rate of this channel does not exceed 10% of the rate of formation of propene (Table 3).

The qualitative shapes of the product branching pressure dependences are best understood by examining the behavior of the k_a parameter (expression VII). k_a, introduced by Rabinovitch and Diesen,[41] presents a convenient means of analysis of falloff curves for chemically activated reactions because it removes from the pressure dependence its dominating Lindemann-type component. While the scale of changes in D/S is comparable with the scale of changing pressure, k_a is less dependent on pressure (all pressure dependence of k_a occurs due to deviation from the Lindemann behavior). The qualitative shapes of the k_a vs pressure dependences obtained in the current work (Figure 5, lower graph) conform to the general trends reported by Rabinovitch et al.[41,75,76] and reanalyzed recently in ref 59. At each temperature, the values of k_a are at a minimum in the middle of the falloff pressure range and increase toward the low- and the high-pressure ends. These increases of k_a at high and low pressures are due to the nonzero widths of the chemical activation energy distribution functions and the multistep character of collisional deactivation, respectively.[59]

Table 3 also presents the values of the rate constants for the two channels of thermal decomposition of propene, reaction 2, calculated using the model of the reaction created in this work (see above). The temperature dependences (900−3000 K) of the high-pressure-limit rate constants of these two channels can be represented with the expressions

$$k^{\infty}_{2a}(T) = 2.49 \times 10^{9}\, T^{2.0} \exp(-46627\ \text{K}/T)\ \text{cm}^3\ \text{molecule}^{-1}\ \text{s}^{-1} \qquad \text{(X)}$$

$$k^{\infty}_{2b}(T) = 5.03 \times 10^{15} \exp(-45374\ \text{K}/T)\ \text{cm}^3\ \text{molecule}^{-1}\ \text{s}^{-1} \qquad \text{(XI)}$$

The relative importance of channels 2a and 2b is a complex function of pressure and temperature. Although one could expect the $H + C_3H_5$ product channel to always dominate at low pressures due to its lower energy barrier (Figure 1), this does not happen (Table 3). As can be seen from the plots in Figure 2, above 2000 K the J-averaged microcanonical rate constants of the $C_2H_3 + CH_3$ product channel (2a, also channel −A in

TABLE 3: Rate Constants and Product Distribution of Reactions 1a, 1b ($C_2H_3 + CH_3$ Combination), 2a, 2b (Thermal Decomposition of Propene), 3a, and 3b ($H + C_3H_5$ Combination) Calculated Using the RRKM/Master Equation Model

P/kPa	*P*/Torr	*T*/K	$k_{1a} + k_{1b}$	S_1[a]	D_1[a]	k_{2a}	k_{2b}	$k_{3a} + k_{3b}$	S_3[a]	D_3[a]
0.1333	1	150	8.2	1.00 (0.00)	0	1.62×10^{-130}	6.24×10^{-114}	1.77	1.00 (0.07)	0.00
1.333	10	150	8.2	1.00 (0.00)	0	1.76×10^{-130}	6.24×10^{-114}	1.78	1.00 (0.03)	0.00
13.33	10^2-10^4	150	8.2	1.00 (0.00)	0	1.78×10^{-130}	6.24×10^{-114}	1.78	1.00 (0.00)	0.00
∞[b]		150	8.2			1.78×10^{-130}	6.24×10^{-114}	1.78		
0.1333	1	310	6.39	0.58 (0.05)	0.42	6.67×10^{-55}	6.22×10^{-48}	1.87	1.00 (0.07)	0.00
1.333	10	310	6.44	0.93 (0.08)	0.07	8.59×10^{-55}	6.23×10^{-48}	1.87	1.00 (0.03)	0.00
13.33	100	310	6.45	0.99 (0.05)	0.01	8.87×10^{-55}	6.23×10^{-48}	1.87	1.00 (0.00)	0.00
133.3	1×10^3	310	6.46	1.00 (0.01)	0	8.90×10^{-55}	6.23×10^{-48}	1.87	1.00 (0.00)	0.00
1333	1×10^4	310	6.46	1.00 (0.00)	0	8.90×10^{-55}	6.23×10^{-48}	1.87	1.00 (0.00)	0.00
∞[b]		310	6.46			8.90×10^{-55}	6.23×10^{-48}	1.87		
0.1333	1	500	6.06	0.24 (0.02)	0.76	5.20×10^{-28}	2.93×10^{-24}	2.06	1.00 (0.08)	0.00
1.333	10	500	6.26	0.73 (0.06)	0.27	9.45×10^{-28}	2.99×10^{-24}	2.14	1.00 (0.06)	0.00
13.33	100	500	6.4	0.95 (0.07)	0.05	1.08×10^{-27}	3.00×10^{-24}	2.15	1.00 (0.02)	0.00
133.3	1×10^3	500	6.44	0.99 (0.02)	0.01	1.10×10^{-27}	3.00×10^{-24}	2.15	1.00 (0.00)	0.00
1333	1×10^4	500	6.44	1.00 (0.00)	0	1.10×10^{-27}	3.00×10^{-24}	2.15	1.00 (0.00)	0.00
∞[b]		500	6.44			1.10×10^{-27}	3.00×10^{-24}	2.15		
0.1333	1	900	5.22	0.02	0.98	5.50×10^{-9}	3.19×10^{-7}	1.24	0.83 (0.07)	0.17
1.333	10	900	5.4	0.19	0.81	1.85×10^{-8}	4.93×10^{-7}	1.95	0.92 (0.08)	0.08
13.33	100	900	5.98	0.59	0.41	3.54×10^{-8}	6.00×10^{-7}	2.43	0.97 (0.06)	0.03
133.3	1×10^3	900	6.66	0.89	0.11	4.53×10^{-8}	6.37×10^{-7}	2.60	0.99 (0.03)	0.01
1333	1×10^4	900	6.97	0.98	0.02	4.80×10^{-8}	6.45×10^{-7}	2.63	1.00 (0.00)	0.00
∞[b]		900	7.05			4.85×10^{-8}	6.46×10^{-7}	2.64		
0.1333	1	1300	4.48	0	1	4.05×10^{-2}	0.329	1.14	0.14	0.86
1.333	10	1300	4.52	0.02	0.98	0.165	0.886	1.44	0.37	0.63
13.33	100	1300	4.78	0.18	0.82	0.492	1.78	1.96	0.64	0.36
133.3	1×10^3	1300	5.66	0.53	0.47	0.980	2.68	2.54	0.85	0.15
1333	1×10^4	1300	6.96	0.85	0.15	1.36	3.22	2.90	0.96	0.04
∞[b]		1300	7.99			1.54	3.43	3.05		
0.1333	1	1800	3.82	0	1	2.78×10^2	3.52×10^2	1.86	0.00	1.00
1.333	10	1800	3.83	0	1	1.14×10^3	1.69×10^3	1.89	0.03	0.97
13.33	100	1800	3.87	0.02	0.98	4.50×10^3	6.11×10^3	1.99	0.12	0.88
133.3	1×10^3	1800	4.14	0.15	0.85	1.42×10^4	1.66×10^4	2.26	0.33	0.67
1333	1×10^4	1800	5.15	0.48	0.52	3.22×10^4	3.31×10^4	2.72	0.64	0.36
∞[b]		1800	8.79			6.24×10^4	5.66×10^4	3.48		
0.1333	1	2400	3.59	0	1	2.76×10^4	3.64×10^3	2.48	0.00	1.00
1.333	10	2400	3.59	0	1	1.26×10^5	4.10×10^4	2.48	0.00	1.00
13.33	100	2400	3.59	0	1	5.78×10^5	2.86×10^5	2.49	0.01	0.99
133.3	1×10^3	2400	3.63	0.02	0.98	2.51×10^6	1.44×10^6	2.52	0.04	0.96
1333	1×10^4	2400	3.89	0.12	0.88	9.06×10^6	5.34×10^6	2.66	0.18	0.82
∞[b]		2400	9.66			5.31×10^7	3.12×10^7	3.94		
0.1333	1	3000	3.64	0	1	3.27×10^5	4.91×10^3	2.84	0.00	1.00
1.333	10	3000	3.64	0	1	1.60×10^6	1.09×10^5	2.84	0.00	1.00
13.33	100	3000	3.64	0	1	7.63×10^6	1.36×10^6	2.84	0.00	1.00
133.3	1×10^3	3000	3.64	0	1	3.60×10^7	1.07×10^7	2.85	0.01	0.99
1333	1×10^4	3000	3.7	0.03	0.97	1.58×10^8	5.99×10^7	2.87	0.04	0.96
∞[b]		3000	10.35			2.72×10^9	1.36×10^9	4.32		

Rate constants units are cm^3 molecule^{-1} s^{-1} and s^{-1}. [a] S_1 and D_1 are the branching fractions of stabilization (formation of thermalized C_3H_6) and decomposition (formation of $H + C_3H_5$ products) in reaction 1. Similarly, S_3 and D_3 are the branching fractions of stabilization (C_3H_6) and decomposition ($C_2H_3 + CH_3$ products) in reaction 3. Values given in parentheses are the branching fractions of formation of cyclopropane and those presented without parentheses correspond to the sum of the C_3H_6 isomers (propene and cyclopropane) [b] Rate parameters given for $P = \infty$ (infinite pressure) are those corresponding to the high-pressure limit. For the chemically activated reactions, stabilization is assumed to be the only important process under the high-pressure-limit conditions. At high temperatures, stabilization will be followed by the fast thermal decomposition of the adduct (reaction 2), which must be taken into account to assess the final distribution of products under particular conditions. Discussion of stabilization followed by thermal reactivation/decomposition is given in section III.4.

Scheme 2) are larger than those of the $H + C_3H_5$ channel (2b, also channel D in Scheme 2) even at low energies due to centrifugal effects (also see subsection III.3). As a result, although channel 2b is the main channel at low temperatures, channel 2a becomes dominant at $T > 2000$ K. It can be noted that the microcanonical variational treatment used here for the $C_3H_6 \rightleftarrows C_2H_3 + CH_3$ channel is essential for the correct description of the competition between channels 2a and 2b and between the reverse decomposition and the further reaction of adduct in the chemically activated reaction 1. A simpler nonvariational approach would neglect the temperature dependence of the centrifugal effects and underestimate the contribution of the $C_3H_6 \rightarrow C_2H_3 + CH_3$ process at high temperatures.

The model of the reaction system $C_2H_3 + CH_3 \rightleftarrows C_3H_6 \rightleftarrows H + C_3H_5$ created in this work was also used to calculate the rate constants and product branching fractions of the reaction

$$H + CH_2CHCH_2 \rightarrow C_3H_6 \quad (3a)$$

$$\rightarrow C_2H_3 + CH_3 \quad (3b)$$

The results are presented in Table 3. As can be seen from the values of the branching fractions, although stabilization (channel 3a) is the main process at low temperatures, decomposition (reaction channel 3b) is increasingly important at temperatures above ~1000 K and becomes dominant above ~2000 K.

III.5. Sensitivity of the Modeling Results to the Uncertainties of the Model. Many of the parameters of the model created

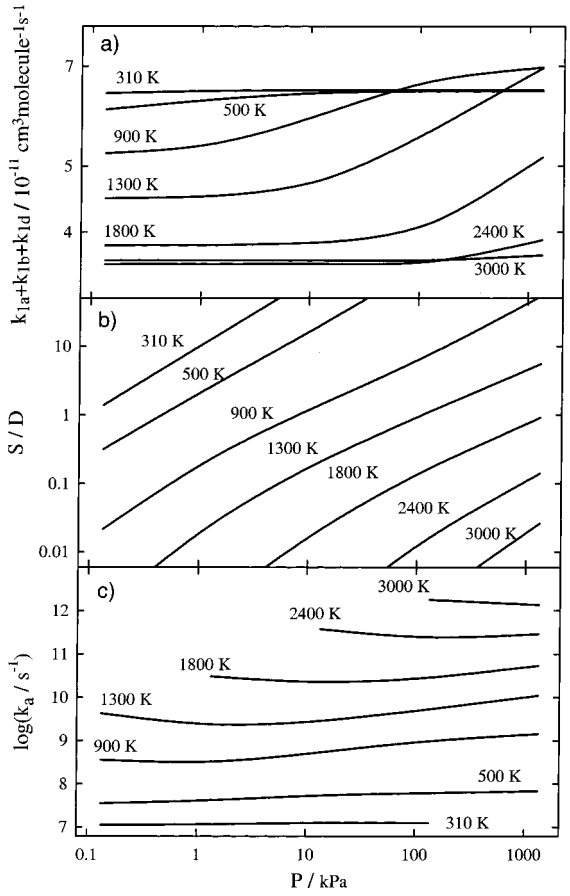

Figure 5. Calculated pressure and temperature dependences of (a) the overall rate constant of the chemically activated (combination) route of reaction 1 ($k = k_{1a} + k_{1b} + k_{1d}$), (b) the stabilization-to-decomposition ratio (S/D = $(k_{1a} + k_{1d})/k_{1b}$), and (c) the "intuitive" rate of decomposition of chemically activated propene, k_a (see text). The $k_a(P)$ dependences that do not cover the whole pressure range on the plot were truncated in order to avoid potential errors associated with very low computed values of stabilization or decomposition branching fractions.

in this study have substantial uncertainties associated with them. The final model is thus not unique in the sense that other values of model parameters (such as properties of the transition states, collisional energy transfer parameters, enthalpies of formation) can be chosen in such a way that the experimental data on the rate constants and branching fractions will still be reproduced. It is impractical to investigate the influence of all model parameter uncertainties on the modeling results because of their large number. However, effects of uncertainties in two of the most important parameters were examined.

One experimental datum which has a large effect on the model properties is the room-temperature rate constant of reaction 3, addition of H atom to allyl radical. The effects of the experimental uncertainty in k_3(298 K) were described in section III.3. Another important parameter to which the modeling results are very sensitive is the energy gap between the barriers for the "entrance" and "exit" channels of the chemically activated reaction. Varying this energy gap in the model has the effect of "shifting" the $k(E)$ dependences along the energy scale relative to the energy distribution of chemically activated adduct and thus modifying the relative efficiency of decomposition vs stabilization.

The parameters that contribute to the uncertainty of this energy gap are the heats of formation of the reactants and products. The experimental uncertainties for the energies of the $C_2H_3 + CH_3$ and $C_3H_5 + H$ channels are ± 4.1 and 2.1 kJ mol^{-1}, respectively (See Table 1.). The $k(E)$ values of these decomposition channels were recalculated for the highest and lowest energies within the uncertainty boundaries of the experimental values. The master equation was, subsequently, solved for the two limiting cases: the energy gap between the two channels is reduced or increased by 6.2 kJ mol^{-1} with respect to the central model. The calculations were performed for conditions corresponding to those of the experimental results of ref 7 at 500 K (pressures of 0.21 and 0.83 kPa, or 1.55 and 6.21 Torr). The S/D (stabilization to decomposition) ratios of the combination route of the $C_2H_3 + CH_3$ reaction obtained with $\langle \Delta E \rangle_{all} = -500$ cm^{-1} for the two limiting cases deviate from the results obtained with the central model: $P = 0.21$ kPa: increased gap $-$ 0.39, decreased gap $-$ 0.64, central model $-$ 0.50; P = 0.83 kPa: increased gap $-$ 1.43, decreased gap $-$ 2.20, central model $-$ 1.77. Reduction in the $\langle \Delta E \rangle_{all}$ value to -640 cm^{-1} for the increased-gap model and increase of $\langle \Delta E \rangle_{all}$ value to -370 cm^{-1} for the decreased-gap model bring the results of the two limiting cases into absolute agreement with the results obtained with the central thermodynamic model and $\langle \Delta E \rangle_{all} = -500$ cm^{-1}. These calculations indicate that, as expected, a strong coupling exists between the "entrance-exit" energy gap and the fitting parameter of the model, $\langle \Delta E \rangle_{all}$. The model, however, shows very little sensitivity to these uncertainties in the thermochemistry, once the $\langle \Delta E \rangle_{all}$ parameter is adjusted to reproduce the experimental data.

When considering practical use of the rate parameters derived in the current study, one should bear in mind that the above model of reactions 1, 2, and 3 is based on significant simplifications. In addition to the sources of uncertainties discussed above, different temperature dependences of the collisional parameters will result in different values of predicted rate constants and branching ratios. Moreover, the simplifications of the model (e.g., assumptions inherent to the formulation of the Master Equation and RRKM method, the representation of the tumbling motion of the C_2H_3, CH_3, and C_3H_5 fragments in transition states with low-frequency vibrational modes, particular shapes of the potential energy profiles of radical−radical addition obtained from quantum chemical calculations) result in uncertainties which are not easily estimated. Therefore, due to the uncertainties of the model, caution is advised in using the results of this modeling and extrapolation far outside the experimental ranges of conditions on the basis of which the model was created.

IV. Summary

The mechanism of the $C_2H_3 + CH_3$ reaction 1 was studied by quantum chemical methods. The results of this study and the analysis of earlier experimental results[5−9] demonstrate that reaction 1 proceeds via two distinctly different routes. The first reaction route is that of radical combination (addition) with the formation of chemically activated propene, which can decompose to H atom and allyl radical (channel 1b) or back to the reactants, isomerize to cyclopropane (1d), or stabilize in collisions with the bath gas (1a). The second route is that of direct abstraction of a hydrogen atom from vinyl radical by the methyl radical (channel 1c, disproportionation).

$$\begin{array}{lcl} & & \text{cyclo-}C_3H_6 \qquad (1d) \\ & & \Updownarrow \\ C_2H_3 + CH_3 & \rightleftarrows & CH_3CHCH_2^* \rightarrow CH_2CHCH_2 + H \qquad (1b) \\ & & \downarrow [M] \\ & & CH_3CHCH_2 \qquad (1a) \end{array}$$

$$C_2H_3 + CH_3 \rightarrow CH_4 + C_2H_2 \qquad (1c)$$

It was demonstrated that the products of channel 1c cannot be produced in the chemically activated reaction route. Other potential channels of reaction 1 forming C_3H_4 isomers were ruled out on the basis of the results of the quantum chemical study.

The abstraction reaction route (1c) proceeds without an energy barrier or with a small barrier. The experimental data of ref 7 demonstrate its negative temperature dependence, which can be represented by the expression

$$k_{1c} = 1.5 \times 10^{-11} \exp(385\ \mathrm{K}/T)\ \mathrm{m^3\ molecule^{-1}\ s^{-1}} \quad \text{(XII)}$$

An RRKM/master equation model of the chemically activated (combination) route of reaction 1 was created on the basis of the results of the quantum chemical calculations and the analysis of experimental data. Microscopic energy- and (for the channel of dissociation to $C_2H_3 + CH_3$) angular momentum-dependent rate constants of barrierless channels of propene dissociation were obtained using a microcanonical variational approach. Potential energy profiles and vibrational frequencies along the reaction paths were calculated for this purpose by quantum chemical methods. Critical parameters of the model (vibrational frequencies of transitional modes and $\langle \Delta E \rangle_{all}$, the average energy transferred per collision with the bath gas) were adjusted to reproduce the experimental data on the high-pressure rate constants of the individual elementary processes involved and on the reaction 1 channel distribution as a function of temperature and pressure. The resultant model provides an extrapolation of the product information obtained in our earlier experimental work[7] to conditions outside of the experimental ranges.

The calculated high-pressure and low-pressure limits of the overall rate constant for the chemically activated route of reaction 1 can be represented by the expressions

$$k^{\infty}_{1a}(T) = 3.51 \times 10^{-12}\, T^{0.417} \exp(161\ \mathrm{K}/T)\ \mathrm{cm^3\ molecule^{-1}\ s^{-1}} \quad \text{(VIII)}$$

$$k^{0}_{1b}(T) = 3.42 \times 10^{-10}\, T^{-0.285}\ \mathrm{cm^3\ molecule^{-1}\ s^{-1}} \quad \text{(IX)}$$

$k^{\infty}_{1a}(T)$ and $k^{0}_{1\,b}(T)$ notations are used here for the high-pressure and the low-pressure-limit rate constants because channels 1a and 1b are the only channels that occur under the corresponding extreme conditions. At temperatures below 500 K and pressures above 1.33 kPa (10 Torr), the formation of propene is the main product channel. Above 2400 K, allyl radical and H-atom are the dominant products. The rate of formation of cyclopropane never exceeds 10% of that of propene. Detailed pressure and temperature dependences of rate constants and product yields are presented in Table 3 and Figure 5.

A byproduct of this analysis of reaction 1 is the models of the reaction of thermal decomposition of propene

$$CH_2CHCH_3 \rightarrow C_2H_3 + CH_3 \quad \text{(2a)}$$

$$\rightarrow H + C_3H_5 \quad \text{(2b)}$$

$$\rightleftarrows \text{cyclo-}C_3H_6 \quad \text{(2c)}$$

and that of H atom with allyl radical

$$H + CH_2CHCH_2 \rightarrow C_3H_6 \quad \text{(3a)}$$

$$\rightarrow C_2H_3 + CH_3 \quad \text{(3b)}$$

The results of the modeling of reaction 2 yield rate constant values that are in agreement with the experimental work of Kiefer et al.[17] The models of reactions 2 and 3 are used to predict the overall rates and product distributions as functions of temperature and pressure. The temperature dependences (900−3000 K) of the high-pressure-limit rate constants of the two channels of reaction 2 can be represented with the expressions

$$k^{\infty}_{2a}(T) = 2.49 \times 10^{9}\, T^{2.0} \exp(-46627\ \mathrm{K}/T)\ \mathrm{s^{-1}} \quad \text{(X)}$$

$$k^{\infty}_{2b}(T) = 5.03 \times 10^{15} \exp(-45374\ \mathrm{K}/T)\ \mathrm{s^{-1}} \quad \text{(XI)}$$

The results of the calculations (Table 3) demonstrate that the relative importance of the channels of reaction 2 changes with temperature: channel 2b is the main one at low temperatures, whereas above 2000 K, channel 2a dominates. For reaction 3, stabilization (3a) is the main process at low temperatures but chemically activated decomposition (3b) is increasingly important at temperatures above ~1000 K and becomes dominant above ~2000 K.

Acknowledgment. This research was supported by Division of Chemical Sciences, Office of Basic Energy Sciences, Office of Energy Research, U.S. Department of Energy under Grant No. DE-FG02-94ER14463. The authors would like to thank Dr. H. Wang for sharing his computational results prior to publication.

Supporting Information Available: Supplement containing a detailed description of the quantum chemical study and details of the rate constant calculations (46 pages). This material is available free of charge via the Internet at http://pubs.acs.org.

References and Notes

(1) Tsang, W.; Hampson, R. F. *J. Phys. Chem. Ref. Data* **1986**, *15*, 1087.
(2) Warnatz, J. *Combustion Chemistry*; Springer-Verlag: New York, 1984.
(3) Gladstone, G. R.; Allen, M.; Yung, Y. L. *Icarus* **1996**, *119*, 1.
(4) Romani, P. N.; Bishop, J.; Bezard, B.; Atreya, S. *Icarus* **1993**, *106*, 442.
(5) Fahr, A.; Laufer, A. H.; Klein, R.; Braun, W. *J. Phys. Chem.* **1991**, *95*, 5, 3218.
(6) Fahr, A.; Braun, W.; Laufer, A. H. *J. Phys. Chem.* **1993**, *97*, 1502.
(7) Stoliarov, S. I.; Knyazev, V. D.; Slagle, I. R. *J. Phys. Chem.* **2000**, *104*, 9687.
(8) Thorn, R. P. Jt.; Payne, W. A., Jr.; Chillier, X. D. F.; Stief, L. J.; Nesbitt, F. L.; Tardy, D. C. *Int. J. Chem. Kinet.* **2000**, *32*, 304.
(9) Fahr, A.; Laufer, A. H.; Tardy, D. C. *J. Phys. Chem.* **1999**, *103*, 8433.
(10) Tardy, D. C.; Rabinovitch, B. S. *J. Chem. Phys.* **1968**, *48*, 5194.
(11) Gilbert, R. G.; Smith, S. C. *Theory of Unimolecular and Recombination Reactions*; Blackwell: Oxford, 1990.
(12) Baer, T.; Hase, W. L. *Unimolecular Reaction Dynamics*; Oxford University Press: New York, 1996.
(13) Holbrook, K. A.; Pilling, M. J.; Robertson, S. H. *Unimolecular Reactions*, 2nd ed.; Wiley: New York, 1996.
(14) Robinson, P. J.; Holbrook, K. A. *Unimolecular Reactions*; Wiley-Interscience: New York, 1972.
(15) Bedanov, V. M.; Tsang, W.; Zachariah, M. R. *J. Phys. Chem.* **1995**, *99*, 11 452.
(16) Knyazev, V. D.; Tsang, W. *J. Phys. Chem. A.* **1999**, *103*, 3944.
(17) Kiefer, J. H.; Al-Alami, M. Z.; Budach, K. A. *J. Phys. Chem.* **1982**, *86*, 808.
(18) Chao, J.; Zwolinski, B. J. *J. Phys. Chem. Ref. Data* **1975**, *4*, 251.
(19) Chase, M. W., Jr.; Davies, C. A.; Downey, J. R., Jr.; Frurip, D. J.; McDonald, R. A.; Syverud, A. N. *JANAF Thermochemical Tables*, 3rd ed.; *J. Phys. Chem. Ref. Data* **1985**, *14*, (Suppl. No. 1).
(20) Pedley, J. B.; Naylor, R. D.; Kirby, S. P. *Thermochemical Data of Organic Compounds*, 2nd ed.; Chapman and Hall: New York, 1986.
(21) Pedley, J. B.; Rylance, J. *Sussex-M. P. L. Computer Analized Thermochemical Data: Organic and Organometallic Compounds*; University of Sussex: Sussex, 1977.

(22) Ervin, K. M.; Gronert, S.; Barlow, S. E.; Gilles, M. K.; Harrison, A. G.; Bierbaum, V. M.; DePuy, C. H.; Lineberger, W. C.; Ellison, G. B. *J. Am. Chem. Soc.* **1990**, *112*, 5750.
(23) Ellison, G. B.; Davico, G. E.; Bierbaum, V. M.; DePuy, C. H. *Int. J. Mass Spectrosc. Ion Proc.* **1996**, *156*, 109.
(24) Böhland, T.; Temps, F.; Wagner, H. G. *Ber. Bunsen-Ges. Phys. Chem.* **1986**, *90*, 468.
(25) Curtiss, L. A.; Raghavachari, K.; Trucks, G. W.; Pople, J. A. *J. Chem. Phys.* **1991**, *94*, 7221.
(26) Pople, J. A.; Gead-Gordon, M.; Raghavachari, K. *J. Chem. Phys.* **1987**, *87*, 5968.
(27) Perdew, J. P.; Wang, Y. *Phys. Rev. B* **1992**, *34*, 13 244.
(28) Becke, A. D. *J. Chem. Phys.* **1992**, *97*, 9173.
(29) Fukui, K. *Acc. Chem. Res.* **1981**, *14*, 363.
(30) Gonzalez, C.; Schlegel, H. B. *J. Phys. Chem.* **1990**, *94*, 5523.
(31) Frisch, M. J.; Trucks, G. W.; Schlegel, H. B.; Scuseria, G. E.; Robb, M. A.; Cheeseman, J. R.; Zakrzewski, V. G.; Montgomery, J. A., Jr.; Stratmann, R. E.; Burant, J. C.; Dapprich, S.; Millam, J. M.; Daniels, A. D.; Kudin, K. N.; Strain, M. C.; Farkas, O.; Tomasi, J.; Barone, V.; Cossi, M.; Cammi, R.; Mennucci, B.; Pomelli, C.; Adamo, C.; Clifford, S.; Ochterski, J.; Petersson, G. A.; Ayala, P. Y.; Cui, Q.; Morokuma, K.; Malick, D. K.; Rabuck, A. D.; Raghavachari, K.; Foresman, J. B.; Cioslowski, J.; Ortiz, J. V.; Stefanov, B. B.; Liu, G.; Liashenko, A.; Piskorz, P.; Komaromi, I.; Gomperts, R.; Martin, R. L.; Fox, D. J.; Keith, T.; Al-Laham, M. A.; Peng, C. Y.; Nanayakkara, A.; Gonzalez, C.; Challacombe, M.; Gill, P. M. W.; Johnson, B.; Chen, W.; Wong, M. W.; Andres, J. L.; Head-Gordon, M.; Replogle, E. S.; Pople, J. A. *Gaussian 98*, revision A.3; Gaussian, Inc.: Pittsburgh, PA, 1998.
(32) Frisch, M. J.; Trucks, G. W.; Schlegel, H. B.; Gill, P. M. W.; Johnson, B. G.; Robb, M. A.; Cheeseman, J. R.; Keith, T.; Petersson, G. A.; Montgomery, J. A.; Raghavachari, K.; Al-Laham, M. A.; Zakrzewski, V. G.; Ortiz, J. V.; Foresman, J. B.; Cioslowski, J.; Stefanov, B. B.; Nanayakkara, A.; Challacombe, M.; Peng, C. Y.; Ayala, P. Y.; Chen, W.; Wong, M. W.; Andres, J. L.; Replogle, E. S.; Gomperts, R.; Martin, R. L.; Fox, D. J.; Binkley, J. S.; Defrees, D. J.; Baker, J.; Stewart, J. P.; Head-Gordon, M.; Gonzalez, C.; Pople, J. A. *Gaussian 94*, revision E.1; Gaussian, Inc.: Pittsburgh, PA, 1995.
(33) Russell, J. J.; Seetula, J. A.; Gutman, D. *J. Am. Chem. Soc.* **1988**, *110*, 3092.
(34) Russell, J. J.; Seetula, J. A.; Senkan, S. M.; Gutman, D. *Int. J. Chem. Kinet.* **1988**, *20*, 759.
(35) Russell, J. J.; Seetula, J. A.; Timonen, R. S.; Gutman, D.; Nava, D. F. *J. Am. Chem. Soc.* **1988**, *110*, 3084.
(36) Chen, Y.; Tschuikov-Roux, E. *J. Phys. Chem.* **1993**, *97*, 3742.
(37) Chen, Y.; Rauk, A.; Tschuikow-Roux, E. *J. Phys. Chem.* **1991**, *95*, 9900.
(38) Chen, Y.; Tschuikow-Roux, E.; Rauk, A. *J. Phys. Chem.* **1991**, *95*, 9832.
(39) Peng, J.; Goumri, A.; Yuan, J.; Marshall, P., manuscript in preparation. Results presented at the 16th International Symposium on Gas Kinetics, Cambridge, UK, July 2000.
(40) Krasnoperov, L. N.; Peng, J.; Marshall, P., manuscript in preparation. Results presented at the 16th International Symposium on Gas Kinetics, Cambridge, UK, July 2000.
(41) Rabinovitch, B. S.; Diesen, R. W. *J. Chem. Phys.* **1959**, *30*, 735.
(42) Miller, H. W.; Handy, N. C.; Adams, J. E. *J. Chem. Phys.* **1980**, *72*, 99.
(43) Baboul, A. G.; Schlegel, H. B. *J. Chem. Phys.* **1997**, *107*, 9413.
(44) Durant, J. L. *Computational Thermochemistry: Prediction and Estimation of Molecular Thermodynamics*; ACS Symposium Series: Washington, DC, 1998.
(45) Beyer, T.; Swinehart D. F. *Comm Assoc. Comput. Machines* **1973**, *16*, 379.
(46) Astholz, D. C.; Troe, J.; Wieters, W. *J. Chem. Phys* **1979**, *70*, 5107.
(47) Knyazev, V. D. *J. Phys. Chem. A* **1998**, *102*, 3916.
(48) Marcus, R. A. *J. Chem. Phys.* **1952**, *20*, 359.
(49) Furue, H.; Pacey, P. D. *Can. J. Chem.* **1982**, *60*, 916.
(50) Pechukas, P. *Dynamics of Molecular Collisions*; Miller, W. H., Ed.; Plenum Press: New York, 1976; Vol. Part B.
(51) Karas, A. J.; Gilbert, R. G.; Collins, M. A. *Chem. Phys. Lett.* **1992**, *193*, 181−184.
(52) Hanning-Lee, M. A.; Pilling, M. J. *Int. J. Chem. Kinet.* **1992**, *24*, 271.
(53) Rabinovitch, B. S.; Tardy, D. C. *J. Chem. Phys.* **1966**, *45*, 3720.
(54) Wilkinson, J. H.; Reinsch, C. *Linear Algebra*; Springer: New York, 1971.
(55) Mokrushin, V.; Bedanov, V.; Tsang, W.; Zachariah, M. R.; Knyazev, V. D. *ChemRate, Version 1.16*; National Institute of Standards and Technology: Gaithersburg, MD 20899, USA, 1999.
(56) Schranz, H. W.; Nordholm, S. *Chem. Phys.* **1984**, *87*, 163.
(57) Smith, S. C.; McEwan, M. J.; Gilbert, R. G. *J. Chem. Phys.* **1989**, *90*, 4265.
(58) Venkatesh, P. K.; Dean, A. M.; Cohen, M. H.; Carr, R. W. *J. Chem. Phys.* **1999**, *111*, 8313.
(59) Knyazev, V. D.; Tsang, W. *J. Phys. Chem. A.* **2000**, *104*, 10 747.
(60) Barker, J. R.; King, K. D. *J. Chem. Phys.* **1995**, *103*, 4953.
(61) Bernshtein, V.; Oref, I. *J. Phys. Chem.* **1993**, *97*, 6830.
(62) Kiefer, J. H.; Kumaran, S. S.; Sundaram, S. *J. Chem. Phys.* **1993**, *99*, 3531.
(63) Kiefer, J. H. *Symp. (Int.) Combust., [Proc.]* **1998**, *27*, 113.
(64) Tsang, W.; Bedanov, V.; Zachariah, M. R. *J. Phys. Chem.* **1996**, *100*, 4011.
(65) Boriesson, L.; Nordholm, S. *Chem. Phys.* **1996**, *212*, 393.
(66) Boriesson, L.; Nordholm, S. *J. Phys. Chem.* **1995**, *99*, 938.
(67) Ming, L.; Sewell, T. D.; Nordholm, S. *Chem. Phys.* **1995**, *199*, 83.
(68) Feng, Y.; Niiranen, J. T.; Bencsura, A.; Knyazev, V. D.; Gutman, D. *J. Phys. Chem.* **1993**, *97*, 871.
(69) Knyazev, V. D. *J. Phys. Chem.* **1995**, *99*, 14 738.
(70) Heymann, M.; Hippler, H.; Troe, J. *J. Chem. Phys.* **1984**, *80*, 1853.
(71) Lim, K. F. *J. Chem. Phys.* **1994**, *101*, 8756.
(72) Knyazev, V. D.; Slagle, I. R. *J. Phys. Chem.* **1996**, *100*, 16 899.
(73) Kiefer, J. H.; Sathyanarayana, R.; Lim, K. P.; Michael, J. V. *J. Phys. Chem.* **1994**, *98*, 12 278.
(74) Dashevskaya, E. I.; Nikitin, E. E.; Oref, I. *J. Phys. Chem.* **1995**, *99*, 9, 10 797.
(75) Kohlmaier, G. H.; Rabinovitch, B. S. *J. Chem. Phys* **1963**, *38*, 1692.
(76) Kohlmaier, G. H.; Rabinovitch, B. S. *J. Chem. Phys* **1963**, *38*, 1709.